

Northumbria Research Link

Citation: Dabrowski, Jessica S., Charette, Matthew A., Mann, Paul, Ludwig, Sarah M., Natali, Susan M., Holmes, Robert Max, Schade, John D., Powell, Margaret and Henderson, Paul B. (2020) Using radon to quantify groundwater discharge and methane fluxes to a shallow, tundra lake on the Yukon-Kuskokwim Delta, Alaska. *Biogeochemistry*, 148 (1). pp. 69-89. ISSN 0168-2563

Published by: Springer

URL: <https://doi.org/10.1007/s10533-020-00647-w> <<https://doi.org/10.1007/s10533-020-00647-w>>

This version was downloaded from Northumbria Research Link:
<http://nrl.northumbria.ac.uk/id/eprint/42318/>

Northumbria University has developed Northumbria Research Link (NRL) to enable users to access the University's research output. Copyright © and moral rights for items on NRL are retained by the individual author(s) and/or other copyright owners. Single copies of full items can be reproduced, displayed or performed, and given to third parties in any format or medium for personal research or study, educational, or not-for-profit purposes without prior permission or charge, provided the authors, title and full bibliographic details are given, as well as a hyperlink and/or URL to the original metadata page. The content must not be changed in any way. Full items must not be sold commercially in any format or medium without formal permission of the copyright holder. The full policy is available online: <http://nrl.northumbria.ac.uk/policies.html>

This document may differ from the final, published version of the research and has been made available online in accordance with publisher policies. To read and/or cite from the published version of the research, please visit the publisher's website (a subscription may be required.)



UniversityLibrary



Northumbria
University
NEWCASTLE

1 *Journal: Biogeochemistry*

2 *Title: Using radon to quantify groundwater discharge and methane fluxes to a shallow,*
3 *tundra lake on the Yukon-Kuskokwim Delta, Alaska*

4 *Authors: Jessica S. Dabrowski* ^{1,2*}, *Matthew A. Charette* ², *Paul J. Mann* ³, *Sarah. M. Ludwig* ⁴, *Susan M.*
5 *Natali* ⁵, *Robert Max Holmes* ⁵, *John D. Schade* ⁵, *Margaret Powell* ⁶, and *Paul B. Henderson* ²

6 ¹ Department of Earth and Planetary Sciences, Massachusetts Institute of Technology, 77 Massachusetts
7 Ave, Cambridge, MA 02139, USA; jsdabrow@mit.edu, *ORCID: 0000-0002-3196-4027*;

8 ² Department of Marine Chemistry & Geochemistry, Woods Hole Oceanographic Institution, 266 Woods
9 Hole Road, MS#25, Woods Hole, MA 02543, USA; mcharette@whoi.edu; phenderson@whoi.edu;

10 ³ Department of Geography & Environmental Sciences, Northumbria University, Newcastle upon Tyne,
11 NE1 8ST, UK; paul.mann@northumbria.ac.uk, *ORCID: 0000-0002-6221-3533*;

12 Department of Earth & Environmental Sciences, Columbia University, 61 Rt. 9W, 207E Oceanography,
13 Palisades, NY 10964, USA; sml2278@columbia.edu; *ORCID: 0000-0002-2873-479X*;

14 ⁵ Woods Hole Research Center, 149 Woods Hole Road, Falmouth, MA 02540, USA; snatali@whrc.org,
15 *ORCID: 0000-0002-3010-2994*; rmholmes@whrc.org, *ORCID: 0000-0002-6413-9154*;

16 jschade@whrc.org;

17 ⁶ Department of Earth and Planetary Sciences, Harvard University, 20 Oxford St, Cambridge, MA 02138,
18 USA; maggiepowell124@gmail.com;

19 * Correspondence: jsdabrow@mit.edu; Tel.: +01-508-289-3850

20 *Abstract:* Northern lakes are a source of greenhouse gases to the atmosphere and contribute substantially to
21 the global carbon budget. However, the sources of methane (CH₄) to northern lakes are poorly constrained
22 limiting our ability to the assess impacts of future Arctic change. Here we present measurements of the natural
23 groundwater tracer, radon, and CH₄ in a shallow lake on the Yukon-Kuskokwim Delta, AK and quantify
24 groundwater discharge rates and fluxes of groundwater-derived CH₄. We found that groundwater was
25 significantly enriched (2000%) in radon and CH₄ relative to lake water. Using a mass balance approach, we
26 calculated average groundwater fluxes of 1.2 ± 0.6 and 4.3 ± 2.0 cm d⁻¹, respectively as conservative and upper
27 limit estimates. Groundwater CH₄ fluxes were 7 - 24 mmol m⁻² d⁻¹ and significantly exceeded diffusive air-
28 water CH₄ fluxes (1.3 – 2.3 mmol m⁻² d⁻¹) from the lake to the atmosphere, suggesting that groundwater is an
29 important source of CH₄ to Arctic lakes and may drive observed CH₄ emissions. Isotopic signatures of CH₄
30 were depleted in groundwaters, consistent with microbial production. Higher methane concentrations in
31 groundwater compared to other high latitude lakes were likely the source of the comparatively higher CH₄
32 diffusive fluxes, as compared to those reported previously in high latitude lakes. These findings indicate that
33 deltaic lakes across warmer permafrost regions may act as important hotspots for CH₄ release across Arctic
34 landscapes.

35 *Keywords:* radon-222; methane; tundra; groundwater; wetland; subarctic;

36 *Acknowledgements:* The authors acknowledge the help of the Polar Field Services Team and helicopter pilot,
37 Stan Herman, for assistance and support in the field. They also thank the other Polaris 2017 and 2018
38 participants for field assistance, ideas, and companionship. J.S.D. thanks Laura Jardine for sharing her soil
39 samples (B2, U1, U3, B3) (Ludwig et al. 2017a) and to Jordan Jimmie for stream discharge data and sampling.
40 This work was funded by National Science Foundation awards OCE-1458305 to M.A.C., 1561437 to S.M.N.,
41 J.D.S., and R.M.H and 1624927 to S.M.N., P.J.M. and R.M.H. We thank the two reviewers for their
42 constructive comments that improved the quality of this manuscript.

43 *1. Introduction*

44 Perennially frozen ground, also known as permafrost, underlies up to 25% of the land in the Northern
45 Hemisphere (Brown et al. 2002). On average, 16% of the terrestrial permafrost landscape is covered by water
46 (Lehner and Döll 2004), and in some areas, like on the Yukon-Kuskokwim Delta in Alaska, it exceeds 30% (US
47 Fish & Wildlife Service 2002). These aquatic systems are closely linked to the terrestrial environment through
48 hydrology. Intense Arctic warming and permafrost thaw may alter the tight connection between terrestrial and
49 aquatic ecosystems. For example, permafrost thaw is causing changes in aquatic systems by changing transit
50 times and shifting flow paths between organic and mineral-rich soils (Vonk et al. 2015).

51 Groundwater is a source of water and solutes to marine and freshwater systems. In temperate and tropical
52 environments, groundwater discharge has been well-documented as a source of nutrients (Charette and
53 Buesseler 2004; Paytan et al. 2006) and carbon (Beck et al. 2007; Richardson et al. 2017; Kim and Kim 2017)
54 to surface waters. In Arctic environments, there are few studies on groundwater discharge, many of which lack
55 information on quantified fluxes of solutes like carbon and nitrogen (see (Lecher 2017) for a review). Permafrost
56 limits most groundwater flow to the shallow, thawed active layer (Williams 1970; Woo 2012). Potential
57 groundwater supply through sediment beds also depends on the presence or absence of continuous permafrost.
58 Taliks—or perennially unfrozen sediments often found beneath lakes and streams—allow for groundwater
59 exchange between a lake and underlying sediments (Woo 2012). Expanding taliks in a warming climate are
60 expected to enhance exchange between lakes, rivers and underlying aquifers via groundwater supply (Walvoord
61 and Kurylyk 2016).

62 Many lakes in polar regions are known to be substantial sources of carbon to the atmosphere ((Wik et al.
63 2016) and references therein), which may be influenced by groundwater-surface water interactions. In addition
64 to delivering dissolved organic carbon that can be mineralized to CO₂ and CH₄, groundwater may directly
65 transport carbon dioxide (CO₂) and methane (CH₄) that was produced in active layer soils to lakes (Kling et al.
66 1992) where CH₄ can be oxidized or released to the atmosphere. Paytan et al. quantified CH₄ transport to a lake
67 in the Arctic suggesting that carbon-rich soils in the northern latitudes, and the release of carbon from permafrost
68 thaw, provide fuel for CH₄ production (Schuur et al. 2008; Natali et al. 2015; Paytan et al. 2015). With the
69 expected shift to greater subsurface flow due to warming combined with future permafrost thaw (Walvoord and
70 Striegl 2007; Bring et al. 2016; Walvoord and Kurylyk 2016), groundwater may become an increasingly
71 important source of CH₄ to lakes in permafrost environments. This is important in the context of the global

72 carbon cycle because lakes in the Arctic constitute a substantial portion of Arctic CH₄ sources and represent
73 6% of global natural CH₄ emissions (Wik et al. 2016).

74 In this study, we investigated the importance of groundwater as a source of CH₄ to a shallow tundra lake.
75 Radon (²²²Rn) was used as a natural geochemical tracer of groundwater discharge (Charette et al. 2008; Dimova
76 and Burnett 2011; Dimova et al. 2013), an approach that is advantageous in regions like northern wetlands
77 because it captures groundwater flow despite their low landscape gradients and microtopographic features that
78 inhibit the use of traditional hydrologic methods such as seepage meters and water table elevation measurements
79 (Morison et al. 2017b). In contrast, ²²²Rn allows for the integration of these heterogeneities. As radon is
80 produced naturally from decay of uranium-series radionuclides in sediments and soils, it is an ideal tracer of all
81 groundwater sources including those present above the permafrost in the seasonally-thawed active layer, in
82 permafrost, and in subpermafrost aquifers (Woo 2012). We used a mass-balance approach (Charette et al. 2008)
83 to quantify groundwater discharge rates and estimate groundwater-derived CH₄ fluxes to the lake and compared
84 them to measured air-water diffusive fluxes and stable isotopes.

85 *2. Materials and Methods*

86 *2.1. Study site*

87 The study site (Fig. 1; 61.264 °N, 163.246 °W) is located 93 km NW of Bethel, AK in the Yukon Delta
88 National Wildlife Refuge (YDNWR). Fieldwork was conducted over two field seasons from July 1 – 13, 2017
89 and June 30 – July 10, 2018. The majority of groundwater and lake sampling was conducted in 2017. Gas
90 exchange coefficients and CH₄ air-water fluxes were measured in 2018. Average air temperatures in this region
91 (1981 – 2010 average for Bethel; US National Weather Service) are -0.8 °C annually, -14.4 °C in January, 13.4
92 °C in July, with above freezing average monthly air temperatures from April to October. Annual precipitation
93 is ~470 mm, with 60 mm occurring in July on average. The average temperatures in July 2017 and 2018,
94 respectively, were 14.4 °C and 13.9 °C. The recorded precipitation in July 2017 was 92 mm and in July 2018
95 was 38 mm (US National Weather Service). The study site is located in a zone of continuous to discontinuous
96 permafrost (Brown et al. 2002) that is moderate in thickness (~180 m) (Ferrians Jr. 1965) with taliks underlying
97 most wetlands and water bodies. Thaw depth was 30 – 40 cm in July 2017 in areas without taliks. The sediments
98 beneath the thick organic layer in this region were deposited in the early Pleistocene (Wilson et al. 2015). This
99 region is characterized by polygonal peat plateaus beside low-lying wetlands. The maximum elevation in this
100 region is approximately 15 meters above sea level and the minimum elevation is approximately 8 m. The
101 elevation of the lake surface and neighboring peat plateaus are 13 and 15 m, respectively.

102 Lakes and ponds occupy about one third of the YDNWR in surface area (US Fish & Wildlife Service
103 2002). Most lakes in this region have a maximum depth of <1-3 m (Bartlett et al. 1992) and range widely in
104 surface area from several square meters to several square kilometers. The lake in this study, colloquially termed
105 “Landing Lake,” has an average depth of 0.53 ± 0.03 m and a surface area of approximately 0.36 km² and is
106 therefore representative of the numerous small, high latitude lakes of the YDNWR. Much of the lake’s
107 watershed is in a region of the YDNWR that experienced a wildfire in 2015, as visible by satellite imagery and
108 evident in the field by a lack of vegetation and the presence of leftover charred materials (Fig. 1). Fire frequency
109 has been found to increase with warming in northern Alaska (Higuera et al. 2011) and on the Yukon-Kuskokwim
110 Delta (Sae-Lim et al. 2019), and can cause permafrost thawing, vegetation shifts, and carbon release (Loranty
111 et al. 2016). Although fire effects were not the focus of this study, statistical tests were performed when enough
112 data was available, and potential implications are discussed (Section 4.1.3). Only one surface water channel
113 was connected to Landing Lake at its southeast corner; it was ~0.33 m wide and ~0.15 m deep, and discharge
114 flowed away from the lake at 0.003 m³ s⁻¹.

115 2.2. *Sample collection*

116 Surface water and groundwater samples for all analyses were collected on July 1 – 12, 2017 and June 30
117 – July 10, 2018 (Fig. 1, Table 1). Samples from active layer soils and lake and pond bottom sediments were
118 collected in 2017 for analysis and incubation experiments in the laboratory. A lake sediment sample
119 (groundwater symbol next to the weather station, Fig. 1) was collected from the top 5 cm using gloved hands,
120 stored in a clean plastic bag, and frozen until analysis (~4 months). Active layer soils ($n = 4$, 0 – 30 cm) were
121 cored using a sharpened steel coring barrel, sample tube and hand drill, and then frozen within 48 hours of
122 collection. Samples were thawed for biogeochemical analyses (available online: (Ludwig et al. 2017a)) ~2
123 weeks after sample collection and refrozen for ~4 months before radionuclide analyses. Air temperature, wind
124 speed and direction, and rainfall rates were collected every 12 minutes using a weather station (AcuRite 5-in-1
125 Weather Sensor) placed ~5 m above the lake surface on a peninsula (Fig. 1). At each surface water and
126 groundwater sampling event, we measured temperature, dissolved oxygen, and electrical conductivity (YSI 6-
127 Series Sonde (2017), YSI ProPlus multiparameter probe (2018)). Instruments were calibrated immediately prior
128 to fieldwork and in the field.

129 Lake water samples (2017, $n = 18$, Table 1) for ²²²Rn were collected in two ways. A RAD AQUA system
130 (Durrige Inc.; (Schubert et al. 2012)) was used for ²²²Rn collection for 17 of the samples. One sample, WP4,
131 was collected in a calibrated 2-L plastic bottle with no headspace that was analyzed within four hours. One 100-

132 L surface water sample (5 20-L “cubitainers”) was collected to estimate ^{222}Rn supported by its parent, ^{226}Ra . At
133 the sampling sites in both years, dissolved CH_4 was collected by vigorously shaking 30-mL of the water sample
134 with 30-mL of ambient air for 60 seconds. The headspace was then transferred into pre-evacuated 12-mL
135 Exetainer vials until slightly over-pressurized. Two separate gas samples were collected for separate analyses
136 of CH_4 concentration and $\delta^{13}\text{CH}_4$, respectively. Samples for water isotope ($\delta^2\text{H}$ and $\delta^{18}\text{O}$) analysis were also
137 collected in 2017 in 4.5-mL glass vials with no headspace.

138 Groundwater samples (2017, $n = 7$, Table 2) were collected from the active layer at 20-40 cm depth below
139 the soil surface using a push-point piezometer (MHE Products, Inc.) and peristaltic pump with gas impermeable
140 tubing. Groundwater samples were limited by the maximum thaw depth of ~40 cm. Samples for ^{222}Rn were
141 collected in 250-mL glass bottles (RAD H2O, DurrIDGE) that were flushed by at least three volumes of sample
142 water and then sealed with no headspace. The same sampling procedures described above for dissolved CH_4
143 and $\delta^2\text{H}$ and $\delta^{18}\text{O}$ isotopes were used for groundwater samples. One set of water samples was also collected
144 from the southeastern stream discharging Landing Lake for CH_4 and water isotopes (Fig. 1, Table 1).

145 Spatial and temporal variation in CH_4 flux was examined across Landing Lake in 2018 to provide context
146 for groundwater fluxes of CH_4 . Seven chambers were deployed for a 24-hour measurement period around the
147 lake. Gas samples from chamber headspace and dissolved surface water were collected upon chamber
148 deployment and after 12-24 hours (Bastviken et al. 2004). Flux rates were calculated from the difference in
149 initial and final concentrations of CH_4 in the chamber, assuming the flux decreased over time in response to a
150 decreasing concentration gradient between the lake water and chamber headspace (Bastviken et al. 2004). To
151 compare the impact of different flux estimate approaches, instantaneous CH_4 fluxes (averaged triplicate
152 measures, each 5 min duration) were measured during the same period. The CH_4 concentrations in the chamber
153 headspace were measured instantaneously using a Los Gatos Research Ultraportable Greenhouse Gas analyzer,
154 and the increase in concentration over the sampling period was used to calculate chamber fluxes by fitting a
155 linear slope to the data.

156 2.3. Sample analysis

157 2.3.1. Radioisotopes

158 Surface water measurements of ^{222}Rn were conducted in two ways. At all lake sampling locations (except
159 WP4) ^{222}Rn was measured using a radon-in-air monitoring system (RAD7, DurrIDGE) connected to a drying
160 unit, spray chamber (RAD AQUA, DurrIDGE, Inc.) and bilge pump. The temperature in the spray chamber was
161 recorded using a stainless-steel temperature probe and data logger (HOBO U12-008, ONSET). At each station,

162 the detector was run for 45 – 75 minutes, including 30 minutes of equilibration. Uncertainties (standard errors)
163 were ~3 – 5% for each sample for the integrated measurement periods. The amount of ^{222}Rn in water was
164 calculated using the measured temperature in the spray chamber and its solubility (Dimova and Burnett 2011).
165 At station WP4, ^{222}Rn was measured in a 2-L sample at the field site using the Big Bottle accessory (Durridge)
166 for the RAD7. The uncertainty or standard error for this method was ~16%.

167 Groundwater ^{222}Rn activities were measured using two different techniques. In the field, groundwater
168 samples ($n = 7$) were analyzed using the RAD H2O accessory (Durridge, Inc.) within 24 hours of collection.
169 Activities were corrected for decay between collection and measurement times. Uncertainties were 9 – 45 %
170 (1σ , standard error). To determine equilibrium ^{222}Rn activities in groundwater as additional endmembers in the
171 model, soils ($n = 4$) and lake sediments ($n = 1$) were incubated in the laboratory (Corbett et al. 1997; Chanyotha
172 et al. 2014). One soil sample (B2, Table 2) was collected >5 km away from the lake, but was included as an
173 endmember due to its similar bulk density to the average bulk density of all other burned soils (Table 3). Radon
174 activities were measured using a radon emanation approach (Key et al. 1979). Efficiencies were determined
175 using a set of radium-fiber standards containing 20 dpm ^{226}Ra (NIST-certified SRM#4967A). Uncertainties
176 were 3 – 15% (1σ , standard error). The ^{222}Rn activities were converted into groundwater endmember activities
177 using porosity and bulk density (Section 2.3.4, Table 3) (Chanyotha et al. 2014).

178 Experiments in the laboratory were carried out with lake bottom sediments to determine the diffusive flux
179 of ^{222}Rn to the lake. Wet sediments were incubated in gas tight flasks with air stones and radium-free water and
180 connected in a closed loop with two charcoal columns as described by Chanyotha et al. (2016). Radon activities
181 were monitored for 10 – 20 hours. The exponential ingrowth of ^{222}Rn activity was linearly approximated (errors
182 of 4 – 10% at 10 – 25 hours) (Chanyotha et al. 2016). This slope was used to calculate the diffusive flux of
183 ^{222}Rn . Leakage of the system over 20 hours was corrected for using a radium-fiber standard containing 20 dpm
184 ^{226}Ra . A second method was used in which lake bottom sediments were incubated and analyzed with the radon
185 emanation approach described above (Key et al. 1979; Corbett et al. 1997; Chanyotha et al. 2014). The total
186 equilibrium ^{222}Rn activity was multiplied by the decay constant and normalized to the area of the flask to obtain
187 an estimate of the diffusive flux of ^{222}Rn to overlying water. The standard error of 3 trials was reported as the
188 uncertainty. Blanks were run using the same experimental setups and subtracted from any reported values.

189 To determine the amount of ^{226}Ra dissolved in the Landing Lake that was supporting ^{222}Rn in the water
190 column, the ~100-L sample was filtered onsite at $<1 \text{ L min}^{-1}$ through a Mn-impregnated acrylic fiber to extract
191 the radium (Moore and Reid 1973). The fiber was analyzed for the activity of ^{222}Rn supported by ^{226}Ra . The

192 fiber was ashed, packed in a polystyrene vial, and sealed with epoxy to prevent ^{222}Rn loss (Charette et al. 2001).
 193 The activity of ^{226}Ra was measured by gamma spectrometry in a well-type germanium gamma detector
 194 (Canberra). The detector was calibrated using a ^{226}Ra standard (NIST-certified SRM#4967A) in the same
 195 geometry as the sample. The standard error (1σ) was reported as the uncertainty in this measurement.

196 Table 1. ^{222}Rn activities and dissolved CH_4 concentrations measured at Landing Lake. Latitude (Lat) and
 197 longitude (Lon) are in decimal degrees. Depth represents depth of water sample collection. Cond. =
 198 conductivity; $\delta^{13}\text{C}$ of methane are presented relative to Pee Dee Belemnite (PDB). H_2O stable isotopes
 199 reported relative to Vienna Standard Mean Ocean Water (VSMOW). Average value \pm standard error is
 200 reported. Stream sample not included in average.

Station	Type	Lat.	Lon.	Depth <i>cm</i>	Cond <i>mS cm⁻¹</i>	O ₂ <i>mg L⁻¹</i>	Water Temp <i>°C</i>	^{222}Rn <i>dpm m⁻³</i>	CH ₄ <i>μmol L⁻¹</i>	$\delta^{13}\text{C}_{\text{CH}_4}$ <i>‰</i>	$\delta^2\text{H}_{\text{H}_2\text{O}}$ <i>‰</i>	$\delta^{18}\text{O}_{\text{H}_2\text{O}}$ <i>‰</i>
WP4	Lake	61.264	-163.246	10	ND ^a	ND	ND	2700	ND	ND	ND	ND
WP6	Lake	61.265	-163.244	45	0.133	14.7	15.7	2640	ND	ND	ND	ND
WP7	Lake	61.263	-163.244	30	0.066	13.7	17.3	1660	ND	ND	ND	ND
WP8	Lake	61.264	-163.243	30	0.051	14.9	15.6	1140	0.1	-45.7	-67.3	-7.5
WP17	Lake	61.268	-163.240	50	0.072	13.9	16.5	1350	1.4	-47.2	-67.1	-7.1
WP18	Lake	61.267	-163.238	50	0.067	10.0	17.4	1370	1.3	-47.1	-67	-7.3
WP19	Lake	61.268	-163.237	43	0.067	10.7	17.7	1051	1.3	-47.0	-67	-7.3
WP20	Lake	61.270	-163.237	40	0.065	9.5	17.9	1390	1.5	-47.3	-67.1	-7.4
WP21	Lake	61.269	-163.241	44	0.062	12.8	18.1	1080	1.5	-46.3	-67.1	-7.3
WP22	Lake	61.268	-163.243	45	0.062	9.2	18.3	1020	1.3	-41.3	-66.9	-7.4
WP31	Lake	61.263	-163.240	35	0.089	10.0	18.3	1620	1.5	-48.0	-65.7	-7.2
WP32	Lake	61.264	-163.239	35	0.087	10.3	18.9	1394	1.8	-44.6	-65.8	-7.2
WP33	Lake	61.265	-163.238	35	0.080	10.4	19.9	1008	1.6	-46.0	-65.7	-7.2
WP34	Lake	61.266	-163.240	50	0.077	11.1	19.4	570	1.5	-48.7	-65.5	-6.5
WP35	Lake	61.267	-163.243	45	0.072	11.1	19.7	1040	1	-49.2	-65.6	-7.3
WP42	Lake	61.267	-163.246	50	0.076	10.5	15.9	1550	1.7	-47.8	-67.5	-7.5
WP46	Lake	61.265	-163.247	40	0.058	10.6	18.9	1640	6.1	-51.4	-68.8	-8.5
WP47	Lake	61.264	-163.248	50	0.059	10.7	18.7	1650	2.9	-48.5	-67.9	-7
Stream	Stream	61.260	-163.241	10	0.020	6.4	8.5	ND	5.5	-47.0	-87.2	-11.5
Avg.					0.073	11.4	17.9	1400	1.8	-47.1	-66.8	-7.3
±					0.004	0.4	0.3	300	0.5	0.6	0.2	0.1

201 ^aND = no data.

202 Table 2. ²²²Rn activities and dissolved CH₄ concentrations measured in groundwater and incubated soils.
 203 Evidence of the 2015 wildfire is noted for each sample. Depth is below the soil surface. Cond. =
 204 conductivity. δ¹³C of dissolved CH₄ are presented relative to Pee Dee Belemnite (PDB). H₂O stable
 205 isotopes reported relative to Vienna Standard Mean Ocean Water (VSMOW). Average value ± standard
 206 error is reported.

Station	Type	Fire ^a	Lat.	Lon.	Depth cm	Cond mS cm ⁻¹	O ₂ mg L ⁻¹	Temp °C	²²² Rn dpm m ⁻³	CH ₄ μmol L ⁻¹	δ ¹³ C _{CH₄} ‰	δ ² H ‰	δ ¹⁸ O ‰
WP5	GW ^b	N	61.263	-163.245	30	ND ^c	ND	ND	48000	ND	ND	ND	ND
WP29	GW	Y/N	61.270	-163.237	30	0.085	2.8	5.1	15000	550.8	-73.6	-94.8	-13.2
WT7-3	GW	Y/N	61.270	-163.237	30	0.030	3.3	3.7	35000	7.8	-50.5	-90.9	-13.1
WP43	GW	Y	61.267	-163.247	30	0.186	5.1	16.8	36000	563.2	-58.0	-95.7	-13.2
WP45	GW	Y	61.265	-163.238	40	0.215	5.7	10.4	29000	612.2	-65.2	-106	-14.6
WP30	GW	N	61.270	-163.239	25	0.118	3.2	10.8	ND	456.2	-50.0	-94.0	-14.0
WT8-2	GW	Y	61.270	-163.236	30	0.043	0.9	12.6	ND	25.1	-73.9	-92.1	-12.9
Bottom	Inc ^d	Y/N	61.264	-163.246	0-5	ND	ND	ND	38000	ND	ND	ND	ND
B2-T1	Inc	Y	61.321	-163.243	0-30	ND	ND	ND	5000	ND	ND	ND	ND
U1-T3	Inc	N	61.258	-163.247	0-30	ND	ND	ND	2000	ND	ND	ND	ND
U3-T1	Inc	N	61.270	-163.237	0-30	ND	ND	ND	1000	ND	ND	ND	ND
B3-T2	Inc	Y	61.271	-163.235	0-30	ND	ND	ND	32000	ND	ND	ND	ND
Avg.						0.113	3.5	9.9	24000	370	-61.9	-95.6	-13.5
±						0.031	0.7	2.0	5000	110	4.4	2.2	0.3

207 ^a Y/N = yes or no for samples collected within the 2015 fire. ^b GW = groundwater. ^c ND = no data. ^d Inc =
 208 Incubated soil or sediment. See ref. (Ludwig et al. 2017a) for more details on soil samples B2, U1, U3 and B3.

209 2.3.2. Methane

210 Methane concentrations were analyzed using a greenhouse gas chromatograph (Shimadzu GC-2014) at
 211 the Woods Hole Research Center, and stable carbon isotopic composition of CH₄ was measured at Northumbria
 212 University using a Delta V Plus IRMS interfaced to a Trace Gas Pre-Concentrator and Gas Bench (Thermo
 213 Scientific). Each isotope measurement run contained three standards (Liso1, Tiso1, Hiso1; Isometric
 214 Instruments), run in full at the beginning and end, with individual standards interleaved throughout (precision
 215 <0.5‰). Both CH₄ concentration and isotopic signatures were blank corrected for atmospheric contamination
 216 assuming the global mean surface atmospheric CH₄ concentration of 1.8 ppm and δ¹³C-CH₄ of -47.2‰
 217 (Warwick et al. 2016) and reported relative to Pee Dee Belemnite (PDB).

218 In 2018, air-water diffusive fluxes (F_{atm}) of CH₄ from the lake were measured directly via the
 219 instantaneous and 24-hr measurement period methods described above. From these data, we calculated the gas
 220 transfer coefficient (k_x) from the following equation:

$$k_x \text{ (m d}^{-1}\text{)} = F_{\text{atm}} \text{ (mol m}^{-1}\text{ d}^{-1}\text{)} / ([X]_{\text{water}} \text{ (mol m}^{-3}\text{)} - [X]_{\text{air}}), \quad (1)$$

221 where [X]_{water} is the measured concentration of dissolved CH₄ in the lake, and [X]_{air} is the concentration of
 222 CH₄ expected in the lake when in equilibrium with the ambient air (Emerson and Hedges 2008). The equilibrium
 223 concentration of CH₄ was calculated using lake temperature, ambient air CH₄ concentration, and Bunsen

224 solubility constants (Wiesenburg and Guinasso 1979). Two models of gas exchange coefficients (k_x)
225 (Crusius and Wanninkhof 2003; Holgerson and Raymond 2016) for the lake was used to derive air-water
226 diffusive fluxes of CH_4 concentrations for Landing Lake in 2017 given similar average wind speed observations
227 for the two years.

228 2.3.3. $\delta^{18}\text{O}$ and $\delta^2\text{H}$

229 To examine hydrologic processes and sources of water into the lake, $\delta^{18}\text{O}$ and $\delta^2\text{H}$ stable isotope values
230 of lake water, stream, and groundwater samples were measured at Northumbria University using a Water
231 Isotope Analyzer (LGR LWIA-24d, San Jose, USA). Ratios were measured to a precision of 0.2‰ for $\delta^2\text{H}$ and
232 0.03‰ for $\delta^{18}\text{O}$ and reported relative to Vienna Standard Mean Ocean Water (VSMOW).

233 2.3.4. Soil characterization

234 Porosity and bulk density were measured in order to calculate equilibrium groundwater radon (^{222}Rn)
235 activities (Table 3) (Chanyotha et al. 2014). Soil and sediment were sampled volumetrically, dried at 60° C
236 (organic soils) or 100° C (sediments) for 48 hours, and bulk densities (B_D) calculated as dry mass/volume.
237 Landing Lake bottom sediment characteristics were averaged for the top 5 cm (measured in 0.5 cm intervals,
238 (Ludwig et al. 2017c)). For porosity measurements, soils and sediments were dried in an oven at 50 °C. Dry
239 sediment/soil was gently packed into a pre-weighed, volume-calibrated test tube. Deionized water was added
240 to the test tube until it just covered the soil surface. The mass of the dry soil and test tube was subtracted from
241 the new mass of the test tube, soil and water. Porosity (ϕ) was then calculated as follows:

$$\phi = [\text{Water added (g)} / \text{Density of water (g cm}^{-3}\text{)}] / \text{Volume of soil (cm}^3\text{)}. \quad (2)$$

242 After measuring the equilibrium ^{222}Rn activities ($A_{222, \text{TOTAL}}$) via radon emanation (see section 2.3.1), the
243 following equation was used to calculate groundwater (GW) ^{222}Rn activities (Chanyotha et al. 2014) :

$$\text{GW } ^{222}\text{Rn (dpm m}^{-3}\text{)} = [A_{222, \text{TOTAL}} / \text{wet mass of soil (g)}] \cdot B_D \text{ (g cm}^{-3}\text{)} \cdot (1 \text{ cm}^3 / 1 \times 10^{-6} \text{ m}^3) / \phi. \quad (3)$$

244 Other soil and sediment characteristics were measured (C, N, moisture, etc.) and can be found online (Ludwig
245 et al. 2017a, c).

246 2.4. Statistical analyses

247 Linear regressions were fit to CH_4 and water stable isotope data with a 99% confidence interval. ANOVAs
248 were used to report *p-values* indicating the significance of the relationship. These analyses were performed

249 across all samples and with the two groups of surface waters and groundwaters, but only statistically significant
 250 relationships ($p < 0.05$) were reported.

251 Although the effects of wildfires on groundwater hydrology and CH₄ are beyond the scope of this study,
 252 statistical tests (t-test, two-sample, unequal variances) were performed with sample data to test the potential
 253 impacts of the 2015 wildfire. First, the relationship between fire and activities of ²²²Rn in groundwater samples
 254 was examined across all groundwater samples taken during the field campaign, including those not adjacent to
 255 Landing Lake (Table 4). The same statistical test was performed for CH₄ in burned and unburned groundwaters.
 256 The impact of fire on soil bulk density was also tested using a two-sample t-test, assuming unequal variances
 257 for soils collected in 2017 (see data online: (Ludwig et al. 2017a)). Only soils from peat plateaus in 2017 were
 258 included to eliminate other environmental variables.

259 Table 3. Measured soil and sediment characteristics used in the incubation experiments. Visible evidence
 260 of the 2015 wildfire is noted for each sample. Sediments were collected from the top 5 cm. Soils were
 261 collected from the 0 - 30 cm. Sample names started with B represent burned soils; U, unburned.

Sample name	Type	Fire in 2015?	Porosity	Dry bulk density <i>g cm⁻³</i>	GW ²²² Rn <i>dpm m⁻³</i>
Bottom Sediment	Landing Lake Sediment	Y/N	0.82	0.45	38000
B2-T1	Soil	Y	0.86	0.19	4800
U1-T3	Soil	N	0.93	0.09	1600
U3-T1	Soil	N	0.90	0.13	1000
B3-T2	Soil	Y	0.74	0.37	32000

262 3. Results

263 Water quality data from Landing Lake and nearby groundwaters are presented in Tables 1 and 2. The
 264 conductivity of surface water and groundwater was on average 0.073 ± 0.004 and 0.113 ± 0.031 mS cm⁻¹,
 265 respectively. All measurements in Landing Lake indicated that it was well oxygenated and thermally well
 266 mixed. The average dissolved oxygen concentration was 11.4 ± 0.4 mg L⁻¹ (115% saturation). Water
 267 temperatures were 15.6 to 19.9 °C with an average of 17.9 °C. Groundwater had a lower average dissolved
 268 oxygen concentration of 3.5 ± 0.7 mg L⁻¹ and a lower average temperature of 9.9 ± 2.0 °C. The stream outlet
 269 of Landing Lake had an intermediate dissolved oxygen concentration of 6.4 mg L⁻¹ and a temperature of 8.5 °C,
 270 which was similar to that of groundwater.

271 3.1. Radioisotopes

272 Radon activities were ~20 times more enriched in groundwater than in surface water samples (Tables 1
 273 and 2). Groundwater samples in burned soils did not significantly differ with respect to ^{222}Rn compared to other
 274 soils ($p = 0.84$, Table 4). However, soils collected in 2017 (see data online: [30]), did significantly differ ($p <$
 275 0.01) in bulk density between recently burned (mean = 0.170 g cm^{-3} , $\sigma^2 = 0.024 \text{ g cm}^{-3}$) and unburned peat
 276 plateaus soils (mean = 0.087 g cm^{-3} , $\sigma^2 = 0.005 \text{ g cm}^{-3}$). In the lake, ^{222}Rn activities were on average $1,400 \pm$
 277 300 dpm m^{-3} (range = $570 - 2,700 \text{ dpm m}^{-3}$) while groundwater activities were $24,000 \pm 5,000 \text{ dpm m}^{-3}$ (range
 278 = $1,000 - 48,000 \text{ dpm m}^{-3}$, Tables 1 and 2). The highest surface water activities were near the southern and
 279 western edges of the lake, and the lowest activities were in the center of the lake (Fig. 2a). The lowest radon
 280 activities in groundwater were for the three soil samples incubated in the laboratory (Table 2). The measured
 281 activity of ^{226}Ra in lake water was $24 \pm 2 \text{ dpm m}^{-3}$ (standard error) and was a minor contributor to the ^{222}Rn
 282 inventory in the lake. The diffusive flux of ^{222}Rn from bottom sediments was $850 \pm 90 \text{ dpm m}^{-2} \text{ d}^{-1}$ and $640 \pm$
 283 $90 \text{ dpm m}^{-2} \text{ d}^{-1}$ as found using the hourly flux method (Chanyotha et al. 2016) and equilibration method (Corbett
 284 et al. 1997), respectively. The average of the two techniques was $740 \pm 140 \text{ dpm m}^{-2} \text{ d}^{-1}$.

285 Table 4. Groundwater samples collected in 2017 (including those near Landing Lake and other lakes) and the
 286 associated ^{222}Rn activities and methane concentrations. Evidence of fire in 2015 is indicated by Y/N.

Sample name	Type	Fire in 2015?	Lat.	Lon.	Depth cm	^{222}Rn dpm m ⁻³	CH ₄ μmol L ⁻¹
WP43	GW ¹	Y	61.267	-163.247	30	36000	563.2
WP45	GW	Y	61.265	-163.238	40	29000	612.2
WT8-2	GW	Y	61.270	-163.236	22	ND ²	25.1
B1-WP27	GW	Y	61.284	-163.247	36	18000	520
B2-WP28	GW	Y	61.273	-163.230	55.5	36000	418.6
B3-WP37	GW	Y	61.284	-163.259	37	19000	ND
B4-WP39	GW	Y	61.284	-163.259	52	32000	628.6
B5-WP40	GW	Y	61.288	-163.262	52	26000	2.9
B2-T1	Inc ³	Y	61.321	-163.243	0-30	4800	ND
B3-T2	Inc	Y	61.271	-163.235	0-30	32000	ND
WP5	GW	N	61.263	-163.245	30	48000	ND
UB1-WP10	GW	N	61.258	-163.246	45	30000	635.3
UB1-WP15	GW	N	61.258	-163.246	36	25000	517.3
UB2-WP25	GW	N	61.321	-163.238	35	65000	98.4
WP30	GW	N	61.270	-163.239	25	ND	456.2
U1-T3	Inc	N	61.258	-163.247	0-30	1600	ND
U3-T1	Inc	N	61.270	-163.237	0-30	1000	ND
Fire, average						26000	395.8
σ^2						1.07×10^8	7.3×10^4
No fire, average						28000	426.8
σ^2						6.39×10^8	5.4×10^4

287 ¹GW = groundwater. ²ND = no data. ³Inc = incubation (See section 2.3.1) for description of incubation
288 methods.

289 3.2. Methane

290 Like radon, dissolved CH₄ was more enriched in groundwater (~200x) than in lake water (Tables 1 and
291 2). Groundwater samples in burned soils did not significantly differ in dissolved CH₄ compared to unburned
292 soils ($p = 0.85$, Table 4). In the lake, CH₄ varied from 0.1 to 6.1 $\mu\text{mol L}^{-1}$ (Fig. 2b) with an average concentration
293 of $1.8 \pm 0.5 \mu\text{mol L}^{-1}$ (Table 1). The highest concentrations were at stations WP46 and WP47 at the southwestern
294 edge of the lake (Fig. 2b). The lowest concentrations were in the center of the lake. Dissolved CH₄
295 concentrations in groundwater varied over a larger range from 8 to 612 $\mu\text{mol L}^{-1}$, and the average groundwater
296 concentration of CH₄ was $370 \pm 110 \mu\text{mol L}^{-1}$ (Table 1). Dissolved CH₄ in the stream was $\sim 5.5 \mu\text{mol L}^{-1}$,
297 intermediate between average lake waters and groundwaters.

298 Dissolved CH₄ in groundwater was on average more depleted in ¹³C than surface water ($-61.9 \pm 4.4\%$ and
299 $-47.1 \pm 0.6\%$, respectively; Tables 1 and 2). The most depleted $\delta^{13}\text{C}$ value of -51.4% in surface water was found
300 at station WP46, coinciding with the highest concentration of CH₄ observed in the lake (Fig. 2b). The stream
301 outlet had a $\delta^{13}\text{C}$ value of -47.0% , similar to lake waters. There was a significant negative relationship between
302 $\delta^{13}\text{C}$ and logged CH₄ concentrations in all samples ($\delta^{13}\text{C} = -5.98 \log [\text{CH}_4, \mu\text{mol L}^{-1}] - 46.9\%$, $R^2 = 0.729$, p
303 < 0.01 , Fig. 3); however, this was largely driven by differences between lake and groundwater samples, and
304 there was no detected relationship between $\delta^{13}\text{C}$ and dissolved CH₄ within each group ($p > 0.01$).

305 In 2018, the average CH₄ concentration in Landing Lake was $1.1 \pm 0.4 \mu\text{mol L}^{-1}$ (Table 6), similar to the
306 average in 2017 of $1.8 \pm 0.5 \mu\text{mol L}^{-1}$. Air-water CH₄ fluxes measured using the instantaneous and 24-hr
307 measurement period methods were $13.5 \pm 3.3 \text{ mmol m}^{-2} \text{ d}^{-1}$ and $2.7 \pm 1.0 \text{ mmol m}^{-2} \text{ d}^{-1}$, respectively. The
308 calculated gas exchange coefficients, k_{600} , using the instantaneous and 24-hr measurement period flux methods
309 were $1.32 \pm 0.50 \text{ m d}^{-1}$ and $0.251 \pm 0.014 \text{ m d}^{-1}$, respectively (Table 6).

310 3.3. $\delta^{18}\text{O}$ and $\delta^2\text{H}$

311 Stable isotopes of H and O in groundwater were more depleted than lake water (Tables 1 and 2, Fig. 4).
312 Lake water $\delta^2\text{H}$ and $\delta^{18}\text{O}$ values were $-66.8 \pm 0.2\%$ and $-7.3 \pm 0.1\%$, respectively, and groundwater $\delta^2\text{H}$ and
313 $\delta^{18}\text{O}$ values were $-95.6 \pm 2.2\%$ and $-13.5 \pm 0.3\%$, respectively. The stream draining Landing Lake had
314 intermediate $\delta^2\text{H}$ and $\delta^{18}\text{O}$ values, respectively, of -87.2% and -11.5% . When $\delta^2\text{H}$ values were plotted as a
315 function of $\delta^{18}\text{O}$ values (Fig. 4), groundwater samples (Table 2) fell close to the Global Meteoric Water Line
316 (Craig 1961), and were represented by following best-fit line: $\delta^2\text{H}_{\text{H}_2\text{O}} = 6.87(\delta^{18}\text{O}) - 2.90\%$ ($R^2 = 0.70$, $p =$

317 0.04). Stable isotope values for all lake and pond samples collected in 2017 (see data online: (Ludwig et al.
318 2017b)) were represented by the following relationship: $\delta^2\text{H}_{\text{H}_2\text{O}} = 4.31(\delta^{18}\text{O}) - 36.55\text{‰}$ ($R^2 = 0.96$, $p \ll 0.01$).
319 Landing Lake surface water samples fell below the GMWL line, but within the range of all lake samples. The
320 stream sample was more depleted than Landing Lake surface waters and was on the line represented by all lakes
321 and ponds.

322 4. Discussion

323 4.1. Radon sources and sinks

324 Consistent with previous studies, ^{222}Rn was much more enriched in groundwater than in surface water
325 (Dimova and Burnett 2011; Dimova et al. 2013; Paytan et al. 2015). Groundwater ^{222}Rn activities (1,000 –
326 48,000 dpm m^{-3}) were less than those observed in sandy, Floridian soils (~170,000 dpm m^{-3}) (Dimova et al.
327 2013) and in silty soils near Toolik Lake, Alaska (~490,000 dpm m^{-3}) (Paytan et al. 2015). The lower activity
328 of ^{222}Rn in soils near Landing Lake was likely due to the organic-rich soils that are low in mineral content (by
329 weight) than most sandy or silty soils and therefore lower in its parent isotope ^{238}U that produces ^{222}Rn . The
330 surface water activities (Fig. 2a, 570 – 2,710 dpm m^{-3}) were similar to those reported in a small lake in Florida
331 (1200 – 4800 dpm m^{-3}) (Dimova and Burnett 2011) and Toolik Lake in Alaska (2900 – 5700 dpm m^{-3}) (Paytan
332 et al. 2015).

333 To quantify groundwater discharge to Landing Lake using ^{222}Rn as a tracer, we constructed a mass balance
334 model that includes all sources and sinks of radon to the lake (Fig. 5). Similar models have been used to study
335 groundwater discharge in both marine and lacustrine environments (Corbett et al. 1997; Dulaiova et al. 2010;
336 Dimova and Burnett 2011; Dimova et al. 2013). The spatial and temporal heterogeneity of groundwater
337 discharge precludes direct quantification; therefore, we use a “flux-by-difference” approach (Charette et al.
338 2008). Assuming steady state over a few weeks, the change in ^{222}Rn over time should be equal to zero, and the
339 sources must be balanced by the sinks:

$$0 = d^{222}\text{Rn}/dt \text{ (dpm } \text{m}^{-2} \text{ d}^{-1}) = F_{222,\text{GW}} + F_{226} + F_{\text{benthic}} - F_{\text{atm}} - \lambda \cdot I_{222} - F_{\text{stream}} - F_{\text{recharge}}. \quad (2)$$

340 The sources in this equation other than groundwater ($F_{222,\text{GW}}$) of ^{222}Rn include alpha-decay of ^{226}Ra in the water
341 column (F_{226}) and diffusive inputs from lake bottom sediments (F_{benthic}). We found no surface water streams
342 entering the lake. The sinks in this model include loss to the atmosphere via gas exchange (F_{atm}), decay ($t_{1/2} =$
343 3.82 days), which is equivalent to the inventory of ^{222}Rn (I_{222}) multiplied by its decay constant ($\lambda = 0.181 \text{ days}^{-1}$),
344 and loss via the stream draining Landing Lake (F_{stream}). Recharge of lake water into downgradient soils and
345 sediments (F_{recharge}) was not measured, although its potential impact on the mass balance is discussed below.

346 Sources of uncertainty for each mass balance model term are described in Table 7. Generally, the largest sources
347 of uncertainty in ^{222}Rn mass balances are natural variability in endmember ^{222}Rn activities and atmospheric
348 evasion, as well as mixing with offshore waters for coastal zones (Burnett et al. 2007).

349 *4.1.1. Sinks of ^{222}Rn : gas exchange, decay, streams, and recharge*

350 To determine the loss of radon via gas exchange, two empirical models were compared to field
351 measurements of the gas exchange coefficient at Landing Lake. The air-water flux of radon was calculated
352 using Equation 1 (Emerson and Hedges 2008). In this case, $[\text{X}]_{\text{water}}$ and $[\text{X}]_{\text{air}}$ are the activities of radon
353 measured in the lake and the activity expected when the lake is in equilibrium with the atmosphere, respectively.
354 We assumed that atmospheric ^{222}Rn was negligible relative to the lake ^{222}Rn ($[\text{X}]_{\text{air}}=0$). The gas exchange
355 coefficient, k_{Rn} , was first estimated based on relationships to temperature (Wanninkhof 1992) and wind speed
356 (Crusius and Wanninkhof 2003). For this mass balance, we used the linear relationship for the SF_6 gas exchange
357 coefficient as a function of wind speed ($0 - 5 \text{ m s}^{-1}$, $20 \text{ }^\circ\text{C}$) for a lake similar in surface area (0.13 km^2) to
358 Landing Lake (0.36 km^2) (Crusius and Wanninkhof 2003). Then, k_{SF_6} ($n = 14$, (Crusius and Wanninkhof 2003))
359 was converted to k_{Rn} for the average water temperature in this study ($17.9 \pm 0.3 \text{ }^\circ\text{C}$) using the appropriate
360 Schmidt numbers ($\text{Sc}(\text{SF}_6, 20 \text{ }^\circ\text{C}) = 956$, $\text{Sc}(\text{Rn}, 20 \text{ }^\circ\text{C}) = 883$, $\text{Sc}(\text{Rn}, 17.9 \text{ }^\circ\text{C}) = 991$) (Wanninkhof 1992;
361 Crusius and Wanninkhof 2003). This resulted in the following best-fit linear relationship as a function of wind
362 speed, u : $k_{\text{Rn}}(17.9 \text{ }^\circ\text{C}, \text{m d}^{-1}) = 0.28 \cdot u(\text{m s}^{-1}) - 0.13$, which had a slope error of 19%, similar to the 20% error
363 that is typical for empirical wind-speed relationships (Dimova and Burnett 2011). We used the average water
364 temperature ($17.9 \pm 0.3 \text{ }^\circ\text{C}$, $n = 18$) and wind speed ($3.83 \pm 0.05 \text{ m s}^{-1}$, $n > 1000$) over the 12-day study period,
365 which resulted in an average gas exchange coefficient of $k_{\text{Rn}} = 1.1 \pm 0.2 \text{ m d}^{-1}$ and atmospheric flux (F_{atm}) of
366 $1,600 \pm 300 \text{ dpm m}^{-2} \text{ d}^{-1}$ (upper limit of gas exchange, Fig. 6).

367 In another study, an empirical relationship based on surface area, rather than wind speed, across 309 small
368 lakes and ponds over a range of latitudes was used to estimate gas exchange (Holgerson and Raymond 2016).
369 To apply this to Landing Lake, we used the gas exchange coefficient for surface areas of $0.1 - 1 \text{ km}^2$ ($k_{600} =$
370 0.80 m d^{-1}) (Holgerson and Raymond 2016) and the Schmidt number for radon at the average lake temperature
371 of $17.9 \pm 0.3 \text{ }^\circ\text{C}$ ($\text{Sc} = 991$) (Wanninkhof 1992) to obtain a second estimate for the gas exchange coefficient of
372 $k_{\text{Rn}} = 0.62 \text{ m d}^{-1}$. This produced a lower estimated atmospheric flux (F_{atm}) of $900 \pm 200 \text{ dpm m}^{-2} \text{ d}^{-1}$ (lower limit,
373 Fig. 6).

374 We compared these literature-derived estimates of the gas transfer coefficient with those obtained from
375 direct measurements of gas exchange in 2018 on Landing Lake via 2-min (instantaneous) and 24-hr

376 measurement floating chambers (Sections 2.2, 2.3.2, Table 6). The coefficients (k_{600} , 12.5 °C) were 1.3 ± 0.5
377 and $0.25 \pm 0.01 \text{ m d}^{-1}$, respectively, according to each method. When the coefficients were converted for radon
378 at the average lake temperature in 2017, it resulted in values of 1.0 ± 0.4 and $0.20 \pm 0.01 \text{ m d}^{-1}$, respectively for
379 k_{Rn} (17.9 °C). CH_4 concentrations and weather conditions were similar in 2017 and 2018, so we expect these
380 gas exchange coefficients to apply to both years. The instantaneous method resulted in gas transfer coefficients
381 similar to the wind speed model, but was likely influenced by ebullition, resulting in overestimates of the
382 diffusive flux, and thus the gas transfer coefficient. The 24-hr measurement period fluxes were less than both
383 the surface area model and wind speed model, which may have been due to the lower temperature of Landing
384 Lake in 2018 compared to 2017 and the shielding of surface water from wind due to the chamber. To encompass
385 uncertainty due to gas exchange in the ^{222}Rn mass balance, we used the surface area model as a conservative
386 estimate and the wind speed model as an upper limit estimate of groundwater fluxes.

387 To calculate radon loss from the lake due to decay, we first estimated the inventory of radon in the lake by
388 multiplying the average depth ($0.53 \pm 0.03 \text{ m}$) by the average activity of ^{222}Rn in the lake ($1400 \pm 300 \text{ dpm m}^{-3}$,
389 Table 1). The flux due to decay is the product of this inventory and the decay constant ($\lambda \cdot I_{222}$), and was equal
390 to $130 \pm 10 \text{ dpm m}^{-2} \text{ d}^{-1}$ (Fig. 6). Of the combined sinks for ^{222}Rn , decay accounted for $8 \pm 1\%$ and $13 \pm 1\%$,
391 while atmospheric exchange was $92 \pm 18\%$ and $87 \pm 17\%$ of total losses of ^{222}Rn , for the upper limit and
392 conservative gas exchange estimates, respectively.

393 We were not able to directly measure the loss of ^{222}Rn due to recharge or the single stream outlet. However,
394 if we assume negligible evaporation and negligible stream outflow to determine the maximum impact of
395 recharge on the mass balance, we expect that lake water would recharge into adjacent wetland areas at the same
396 rate as groundwater influx ($\sim 1 - 4 \text{ cm d}^{-1}$) with a ^{222}Rn activity equal to average lake water (1400 dpm m^{-3}). The
397 ^{222}Rn loss rate for this process would be $20 - 60 \text{ dpm m}^{-2} \text{ d}^{-1}$, or only 2 – 3% of the combined losses due to
398 decay and gas exchange. In the case of the stream outlet, discharge was $\sim 0.003 \text{ m}^3 \text{ s}^{-1}$, which is equivalent to
399 0.07 cm d^{-1} when integrated over the lake's area, as with the other mass balance terms. If the ^{222}Rn activity of
400 the stream is assumed to be that of average lake water (1400 dpm m^{-3}), then the ^{222}Rn loss would be 1.0 dpm m^{-2}
401 d^{-1} , or 0.06 – 0.10% of the combined sinks of decay and gas exchange. Therefore, both recharge and the stream
402 outlet are considered negligible sinks in the ^{222}Rn mass balance, well within the uncertainty of most of the model
403 terms (Table 7).

404 *4.1.2. Sources of ^{222}Rn : dissolved ^{226}Ra , sediments, groundwater*

405 Potential sources of ^{222}Rn in this system other than groundwater are production via decay of dissolved
406 ^{226}Ra and diffusive inputs from bottom sediments (Fig. 5). We first calculated the dissolved inventory of ^{226}Ra
407 by multiplying the measured activity of ^{226}Ra in the lake (24 dpm m^{-3}) by the average depth (0.53 m). The
408 inventory of ^{222}Rn supported by ^{226}Ra is equivalent to the dissolved inventory of ^{226}Ra ($12 \pm 1 \text{ dpm m}^{-2}$)
409 multiplied by the decay constant of ^{222}Rn . This results in a flux (F_{226}) of $30 \pm 2 \text{ dpm m}^{-2} \text{ d}^{-1}$ (Fig. 6). In our
410 steady state model where we assume that sources are equal to sinks, the input of ^{222}Rn from ^{226}Ra can only
411 account for 2 – 3% of the radon inputs to the lake, consistent with other lake ^{222}Rn budgets (Corbett et al. 1997;
412 Dimova et al. 2013).

413 The diffusive input of ^{222}Rn , which was measured in the laboratory using Landing Lake sediments, agreed
414 well between the two methods. The short-term measurement over 10 – 20 hours resulted in a greater flux than
415 the equilibration method, likely due to the larger concentration gradient between sediment and overlying water
416 for shorter incubation periods. Because the short-term measurement approximates the decay as a linear function,
417 up to 10% error is expected in addition to any experimental error. In the mass balance, we used the average of
418 the two techniques ($740 \pm 140 \text{ dpm m}^{-2} \text{ d}^{-1}$) for the sediment-water diffusive flux (Fig. 6). The flux was less than
419 that of freshwater lake sediments from Cambodia ($2040 \text{ dpm m}^{-2} \text{ d}^{-1}$) (Chanyotha et al. 2016), although this is
420 expected because radon is derived from natural uranium in minerals (Charette et al. 2008), and the lake
421 sediments in the YDNWR have a low mineral content. The ^{222}Rn diffusive flux accounted for 42 and 72% of
422 sources in the radon budget for the upper limit and conservative estimates, respectively (Fig. 6). This
423 contribution from diffusion is higher than most lake budgets (Dimova et al. 2013, 2015); since Landing Lake is
424 only ~0.5 m deep, the ratio of bottom sediment area to lake volume is relatively large, which likely explains
425 why diffusion is estimated to be a major contributor to the Landing Lake ^{222}Rn inventory.

426 Together, diffusive inputs and dissolved ^{226}Ra decay account for 44 to 73% of the sources in the mass
427 balance. Assuming negligible transport of ^{222}Rn out of Landing Lake via recharge and streams (Section 4.1.1),
428 groundwater must be the missing source that contributes 27 to 56% of radon to the lake inventory (Fig. 6).

429 4.1.3. *Quantifying groundwater fluxes*

430 With measurements of groundwater endmembers, one can convert the ^{222}Rn fluxes into groundwater fluxes
431 and volumetric discharge estimates. The remaining 25 ± 10 to $58 \pm 24\%$ of the ^{222}Rn inventory was 300 ± 100
432 to $1000 \pm 400 \text{ dpm m}^{-2} \text{ d}^{-1}$, for the conservative and upper limit estimates, respectively (Fig. 6). In the following
433 equation (Charette et al. 2008),

$$F_{GW} \text{ (m d}^{-1}\text{)} = F_{222,GW} \text{ (dpm m}^{-2} \text{ d}^{-1}\text{)} / A_{GW} \text{ (dpm m}^{-3}\text{)}, \quad (3)$$

434 $F_{222,GW}$ is the flux of ^{222}Rn via groundwater and A_{GW} is the activity of ^{222}Rn in groundwater. There is a
 435 significant amount of variability in the groundwater samples when considering both field samples and
 436 incubations. ^{222}Rn activities in groundwater at Landing Lake are likely controlled by the mineral content of soils,
 437 which is known to increase with depth in peatlands (Morison et al. 2017a). Using the average endmember (Table
 438 2, $24,000 \pm 5,000 \text{ dpm m}^{-3}$), the ^{222}Rn flux via groundwater (300 ± 100 to $1000 \pm 400 \text{ dpm m}^{-2} \text{ d}^{-1}$) and Equation
 439 3, we calculated groundwater fluxes of 0.012 ± 0.006 and $0.043 \pm 0.020 \text{ m d}^{-1}$ (1.2 ± 0.6 , $4.3 \pm 2.0 \text{ cm d}^{-1}$, Table
 440 5), respectively, for conservative and upper limit estimates. If we use the highest activity endmember ($48,000$
 441 dpm m^{-3}), the groundwater flux is 0.6 ± 0.3 to $2.1 \pm 0.9 \text{ cm d}^{-1}$ (Table 5), for conservative and upper limit
 442 estimates, respectively. Since these groundwater fluxes were calculated using the average ^{222}Rn inventory for
 443 the whole lake surface, they represent inflow averaged over the lake's area. We only have one sample for lake
 444 bottom sediment porewater ($^{222}\text{Rn} = 38,000 \text{ dpm m}^{-3}$) that may be representative of possible subpermafrost
 445 groundwater, which is higher in activity than the average groundwater endmember. If subpermafrost
 446 groundwater were a significant source of water to this lake, it would likely have a ^{222}Rn activity similar to that
 447 of our porewater sample, which is greater than our average groundwater endmember but less than the highest
 448 activity endmember; therefore, it would not impact our estimate of ^{222}Rn -based groundwater discharge fluxes.
 449 Another factor that could influence these groundwater fluxes is the impact of the 2015 wildfire. Fire did not
 450 seem to have a significant impact on ^{222}Rn activities in groundwater, but it did result in significantly higher bulk
 451 densities (Table 3). Higher soil density usually lowers hydraulic conductivity, which could cause the
 452 groundwater fluxes to be lower in fire-affected areas of the watershed. A dedicated process study would be
 453 needed to truly determine the environmental impacts of fire on groundwater hydrology.

454 The volumetric input of groundwater to the lake of $4,000 \pm 2,000$ to $15,000 \pm 7000 \text{ m}^3 \text{ d}^{-1}$ was estimated
 455 by multiplying the groundwater flux (1.2 ± 0.6 to $4.3 \pm 2.0 \text{ cm d}^{-1}$) by the lake area ($3.6 \times 10^5 \text{ m}^2$). Such a
 456 discharge rate would flush the lake about 3 – 7% by volume per day, equivalent to a residence time of 15 – 53
 457 days (Table 2). For lakes in the US with depths $<2 \text{ m}$, residence times on average are 30 – 300 days (Brooks et
 458 al. 2014), which agrees well with the residence times calculated here.

459 Table 5. Estimates of groundwater fluxes, residence times, and methane fluxes for Landing Lake
 460 compared to other studies. Average and high activity endmembers refer to the concentrations of radon in
 461 groundwater.

Lake name	GW ^a flux <i>cm d⁻¹</i>	Residence time <i>days</i>	GW [CH ₄] ^b <i>μmol L⁻¹</i>	GW CH ₄ flux <i>mmol m⁻² d⁻¹</i>	Lake [CH ₄] <i>μmol L⁻¹</i>	Air-water CH ₄ flux ^c <i>mmol m⁻² d⁻¹</i>
Landing Lake average endmember	1.2 ± 0.6 to 4.3 ± 2.0	12 – 44	370 (8 - 612)	4 ± 2 to 16 ± 7	1.8 ± 0.3	1.3 – 2.3 (1.3 – 5.7)
Landing Lake high activity endmember	0.6 ± 0.3 to 2.1 ± 0.9	25 – 88	370 (8 - 612)	2 ± 1 to 8 ± 3	1.8 ± 0.3	1.3 – 2.3 (1.3 – 5.7)
Toolik Lake (Paytan et al. 2015; Garcia-Tigreros Kodovska et al. 2016)	1.4 ± 0.9	ND ^d	8 – 35 (0.01 – 150)	0.1 – 0.7	0.02 – 0.8	0.06 – 0.2
Northern peatland ponds (n = 38) (Wik et al. 2016)	ND	ND	ND	ND	ND	7 (2 – 10)

462 ^a GW = groundwater. ^b Average listed along with minimum and maximum in parentheses. Other values listed
463 with entire range of estimates or as average ± standard deviation. ^c Estimated air-water fluxes calculated using
464 Equation 1 and measured air-water fluxes via 24-hr measurement period flux chambers in 2018 listed in
465 parentheses. See Table 6 in Appendix for details. ^d ND = no data.

466 Unless the lake volumes were increasing over the study period, any groundwater inputs to the lake must
467 be lost to surface water flow, wetland recharge, or evaporation. Surface water flow was estimated to drain only
468 0.5% of Landing Lake's volume per day, and we had no means to quantify recharge from the lake to the
469 subsurface. If the talik beneath the lake does not penetrate the permafrost completely, the main recharge pathway
470 for water flow would be through the wetland areas near the lake, visible as a darker green color just north and
471 west of the lake (Fig. 1), or through outlet streams. The elevation difference between the plateaus and low-lying
472 areas, such as the lake surface and wetlands, was approximately 2 meters, likely enough to support some level
473 of hydrologic outflow.

474 Stable isotopes ($\delta^{18}\text{O}$ and $\delta^2\text{H}$ of H_2O) provide quantitative evidence for evaporation at Landing Lake
475 (Fig. 4). All lakes and ponds sampled in 2017 (Ludwig et al. 2017b) fall on the following best-fit line: $\delta^2\text{H}_{\text{H}_2\text{O}}$
476 = 4.31($\delta^{18}\text{O}$) – 36.55‰ ($R^2 = 0.96$), which we define as the Local Evaporation Line (LEL). A slope of 4.31 is
477 within modeled slopes of 4 – 6 for lakes at 60°N (Gibson et al. 2008) and measured slopes of 4.1 – 7.1 in
478 Canadian lakes and wetlands (Gibson et al. 2005). Landing Lake surface waters fell on the LEL and seem to be
479 more impacted by evaporation than the majority of the lakes and ponds sampled, which is expected since
480 Landing Lake had the highest surface area and a similar depth compared to the other sampling sites. The
481 intersection of this evaporation line with the meteoric water line indicates the source of water to the lake (Fontes
482 1980) was locally sampled active layer groundwaters. Stable isotopes in groundwaters were close to the GMWL
483 and therefore were similar to precipitation. Another study of water stable isotopes in also found that summer
484 precipitation was the major source of water to the active layer on the Alaskan tundra (Throckmorton et al. 2016).

485 These data show that evaporation was a significant loss of water during the study period, although the exact
486 percentage is not quantifiable with the available data.

487 4.2. Methane in Landing Lake

488 Using the radon-derived groundwater fluxes ($F_{\text{GW}} = 1.2 \pm 0.6$ to 4.3 ± 2.0 and 0.6 ± 0.3 to 2.1 ± 0.9 cm d⁻¹)
489 and dissolved CH₄ concentration measurements, we estimated groundwater fluxes of CH₄ to Landing Lake
490 from the following equation,

$$F_{\text{CH}_4, \text{GW}} (\text{mmol m}^{-2} \text{ d}^{-1}) = F_{\text{GW}} (\text{m d}^{-1}) \cdot [\text{CH}_4]_{\text{GW}} (\text{mmol m}^{-3}), \quad (4)$$

491 in which $F_{\text{CH}_4, \text{GW}}$ is the flux of CH₄ to Landing Lake via groundwater, and $[\text{CH}_4]_{\text{GW}}$ is the concentration of
492 CH₄ in groundwater (average = 370 $\mu\text{mol L}^{-1}$). The groundwater flux of CH₄ to Landing Lake ($F_{\text{CH}_4, \text{GW}}$) for
493 July 2017 was 4 ± 2 to 16 ± 7 $\text{mmol m}^{-2} \text{ d}^{-1}$ (High ²²²Rn endmember: 2 ± 1 to 8 ± 3 $\text{mmol m}^{-2} \text{ d}^{-1}$, Table 5). A
494 study at Toolik Lake, AK conducted during July in 2011 and 2012, the same time of year as this study, included
495 similar methods to determine radon-derived groundwater fluxes (Paytan et al. 2015). The groundwater flux of
496 CH₄ to Landing Lake is an order of magnitude greater than to Toolik Lake (Table 5, 0.1 – 0.7 $\text{mmol m}^{-2} \text{ d}^{-1}$),
497 despite having similar groundwater fluxes (Table 5, 1.2 ± 0.6 to 4.3 ± 2.0 cm d⁻¹ at Landing Lake; 0.5 – 2.3 cm
498 d⁻¹ at Toolik Lake). This is largely due to the greater Landing Lake groundwater CH₄ concentrations (370 μmol
499 L^{-1}) compared to Toolik (21 $\mu\text{mol L}^{-1}$). These higher fluxes may lead to the observed higher surface water
500 dissolved CH₄ in Landing Lake than at Toolik (Table 5, 1.8 ± 0.3 $\mu\text{mol L}^{-1}$ and 0.02 – 0.8 $\mu\text{mol L}^{-1}$,
501 respectively). A fraction of CH₄ measured in groundwaters may be oxidized before reaching lake surface
502 waters, and other sources of CH₄, such as methanogenesis in lake sediments may drive the observed differences.
503 Further investigation is recommended to confirm the role that groundwater plays in CH₄ lake budgets.

504 The depleted carbon-isotopic signature of CH₄ in groundwater ($-61.9 \pm 4.4\%$, Table 2) is consistent with
505 microbial production (Hornibrook et al. 1997; Whiticar 1999), and the large range in isotopic values suggests
506 both methanogenesis and oxidation may be occurring. If oxidation is a dominant process removing CH₄, it is
507 expected that $\delta^{13}\text{C}$ will increase logarithmically as CH₄ decreases because lighter CH₄ is preferred in the
508 reaction (Whiticar and Faber 1986; Whiticar 1999), a pattern which was observed in Landing Lake between
509 groundwater and lake water samples (Fig. 3). We assume that the highest concentration of CH₄ observed in
510 groundwater was the starting concentration and stable isotopic composition before any oxidation ($[\text{CH}_4]_{\text{GW}} =$
511 $612 \mu\text{mol L}^{-1}$, $\delta^{13}\text{C}_{\text{CH}_4, \text{GW}} = -65.2\%$, Table 2). The final composition after oxidation was assumed to be the
512 average concentration and stable isotope value in Landing Lake ($[\text{CH}_4]_{\text{LAKE}} = 1.8 \mu\text{mol L}^{-1}$, $\delta^{13}\text{C}_{\text{CH}_4, \text{LAKE}} = -$
513 47.1% , Table 1). Following the equation below (Whiticar and Faber 1986):

$$\delta^{13}\text{C}_{\text{CH}_4, \text{LAKE}} = [\delta^{13}\text{C}_{\text{CH}_4, \text{GW}} + 1000([\text{CH}_4]_{\text{LAKE}} / [\text{CH}_4]_{\text{GW}})^{1/\alpha-1}] - 1000, \quad (5)$$

514 The fractionation factor (α) between starting groundwater CH_4 and average lake CH_4 was 1.003, in good
 515 agreement, considering the margin of error, with the expected α of 1.005 – 1.030 for bacterial CH_4 oxidation
 516 (Whiticar 1999), which supports the idea that CH_4 in the lake was produced in the active layer and then
 517 transported by groundwater movement, as has been qualitatively observed in other lakes and streams (Kling et
 518 al. 1992; Crawford et al. 2013).

519 Additionally, CH_4 produced in bottom sediments may also be transported into the lake by diffusion and
 520 ebullition. Additional measurements of CH_4 concentrations and $\delta^{13}\text{C}_{\text{CH}_4}$ in sediment porewater profiles and
 521 floating chambers would be necessary to completely quantify sediment-water diffusive fluxes and ebullitive
 522 fluxes, respectively, and their contribution to the lake's CH_4 budget. Diffusion, ebullition and advection may
 523 collectively contribute to the CH_4 budget, and each may be impacted by environmental changes. As
 524 precipitation increases in the Arctic (Rawlins et al. 2010; Wrona et al. 2016), groundwater flow is expected to
 525 increase, impacting advective transport of CH_4 (Walvoord and Kurylyk 2016). Recent work has also revealed
 526 that abrupt thaw beneath Arctic lakes can accelerate carbon emissions from lakes (Walter Anthony et al. 2018),
 527 potentially increasing future diffusive and ebullitive CH_4 fluxes from sediments.

528 Once CH_4 enters a lake, it may be lost in the water column via oxidation, to the atmosphere by gas
 529 exchange, to groundwater recharge, or surface transport. We calculated diffusive air-water CH_4 (Section 2.3.2),
 530 using the observed ($1.8 \pm 0.3 \mu\text{mol L}^{-1}$) and saturated concentrations of CH_4 in the lake ($0.004 \mu\text{mol L}^{-1}$) and
 531 two modeled gas exchange coefficients ($k_{\text{CH}_4} = 1.36 \text{ m d}^{-1}$ and 0.79 m d^{-1} , at $17.9 \text{ }^\circ\text{C}$). The flux from Landing
 532 Lake to the atmosphere for July 2017 was $1.3 - 2.3 \text{ mmol m}^{-2} \text{ d}^{-1}$, approximately 3 – 18 times less than lake
 533 input of CH_4 via groundwater (Table 5). The 24-hr measurement period CH_4 fluxes in 2018 were $1.3 - 5.7$
 534 $\text{mmol m}^{-2} \text{ d}^{-1}$ (Tables 5 and 6), which agreed well with the calculated diffusive air-water fluxes. This suggests
 535 that groundwater sources of CH_4 can support all observed diffusion of CH_4 from the lake surface and that they
 536 may be a driver of observed diffusive CH_4 emissions.

537 That the groundwater fluxes of CH_4 were higher than air-water diffusive losses is likely due to the
 538 additional removal of CH_4 via oxidation in the water column (Whiticar 1999; Bastviken et al. 2002), a
 539 determination supported by $\delta^{13}\text{C}_{\text{CH}_4}$ (Fig. 3). Oxidation of CH_4 in the water column of freshwater lakes is
 540 expected by CH_4 oxidizing bacteria (Whiticar 1999) and is typically 30 – 99% of CH_4 produced in sediments
 541 or anoxic waters (e.g. (Bastviken et al. 2002, 2008)). Typical oxidation rates can therefore account for this
 542 “missing” CH_4 in Landing Lake. Climate warming will increase both methanogenesis and CH_4 oxidation, but

543 oxidation rates are typically less temperature dependent than production rates, and lower solubility of CH₄ in
 544 warmer waters may cause CH₄ release via bubbles that escape oxidation (Dean et al. 2018).

545 The air-water diffusive flux in this study was similar to the diffusive methane flux of 2 – 10 mmol m⁻² d⁻¹
 546 for 38 peatland ponds across the Arctic and subarctic (Table 5) (Wik et al. 2016). Another study of 40 lakes in
 547 Alaska (~65°N) with similar surface areas found average air-water CH₄ fluxes in summer of 0.6 mmol m⁻² d⁻¹
 548 (Sepulveda-Jauregui et al. 2015). It is important to note that this study was done in the summer season, so these
 549 fluxes are likely to change with better temporal coverage. Polar regions are expected to become warmer (Schuur
 550 et al. 2008, 2015; Vihma et al. 2016) and wetter (Rawlins et al. 2010; Wrona et al. 2016) over the following
 551 decades, so higher CH₄ production in soils is expected if increasing precipitation increases soil moisture (Natali
 552 et al. 2015) which can then be transported to aquatic systems by groundwater flow.

553 In this study, we used naturally occurring ²²²Rn to quantify groundwater discharge and dissolved CH₄
 554 fluxes to a lake in a subarctic terrestrial wetland. Groundwater fluxes were similar to those at another lake in
 555 Alaska measured with the same radon-budget method (Paytan et al. 2015). We found that groundwater is a
 556 source of CH₄ to the lake as suggested by the fact that groundwater CH₄ fluxes substantially exceeded diffusive
 557 fluxes from the lake surface. The concentrations of CH₄ and diffusive fluxes were higher than the well-studied
 558 Toolik Lake. Increased CH₄ production with warming and wetting of the Arctic may lead to higher rates of
 559 delivery of CH₄ to aquatic environments due to the combined increase in CH₄ production (Natali et al. 2015)
 560 and the shift to greater subsurface flow as permafrost thaws (Walvoord and Kurylyk 2016).

561 *Appendix 1: Methane fluxes*

562 Table 6. The methane concentrations, measured fluxes, and measured gas exchange coefficients for
 563 Landing Lake, July 2018. Each method is described in Section 2.2. Average wind speed over the 3 days
 564 was 4.6 ± 1.1 m s⁻¹. All measurements were made at the same location (latitude, longitude): 61.26583, -
 565 163.24199.

Sample	Method	Length of deployment	Temp. °C	Lake CH ₄ μmol L ⁻¹	CH ₄ flux mmol m ⁻² d ⁻¹	k ₆₀₀ m d ⁻¹
7_8	24-hr period	3.6 hr	13.3	2.35	5.7	0.24
7_8	Instantaneous	15 min	13.3	2.35	21.8	0.93
7_9	24-hr period	28.7 hr	12.1	0.93	2.0	0.23
7_9	Instantaneous	15 min	12.1	0.93	6.3	0.71
7_10A	24-hr period	16.6 hr	11.6	0.65	1.8	0.29
7_10A	Instantaneous	15 min	11.6	0.65	17.1	2.32
7_10B	24-hr period	21.4 hr	12.7	0.58	1.3	0.24
7_10B	Instantaneous	15 min	12.7	0.58	17.0	ND ^a
7_10C	Instantaneous	15 min	13.7	ND	5.1	ND

24-hr measurement period average	12.4	1.1	2.7	0.251
±	0.7	0.8	1.0	0.014
Instantaneous average	12.7	1.1	13.5	1.32
±	0.9	0.8	7.4	0.50

566

^aND = no data.

567 *Appendix 2: Uncertainty estimates in the mass balance model*

568 Table 7. The parameters in the mass balance and the methods for estimating the uncertainty in each

569 parameter.

Parameter	Estimation of uncertainty
Gas exchange, Wind Speed Model	Slope error (19%); standard deviation of measured wind speeds (<1%, n > 1000)
Gas exchange, Size Class Model	Estimated at 20% (std error = 7-25% in Holgerson & Raymond, 2016)
Gas exchange, direct measurement	Standard error of measurements (24-37%)
Gas exchange in mass balance	Two estimates: Conservative = Size Class, Upper Limit = Wind Speed; Both errors ~20%
Decay	Standard error of lake ²²² Rn inventories (11%, n = 18)
Recharge	Impact on mass balance discussed in Section 4.1.1
Stream discharge (out of lake)	Impact on mass balance discussed in Section 4.1.1
Diffusion from bottom sediments	Propagated measurement error of the two methods (19%)
Dissolved ²²⁶ Ra	Measurement error of ²²⁶ Ra by gamma spectrometry (8%)
Groundwater ²²² Rn flux	Propagated uncertainty of all model terms (41%)
Groundwater flux (cm d ⁻¹)	Reported range for each estimate propagated from: 1) uncertainty of the ²²² Rn flux (41%); 2) standard error in average groundwater endmember (21%, n = 10) OR measurement error in high activity groundwater endmember (8%)

570 *Author Contributions:* Conceptualization, J.S.D., M.A.C., R.M.H, S.M.N, J.D.S. and P.J.M.; methodology,
571 J.S.D., M.A.C. P.J.M., and S.M.L.; validation, J.S.D. and M.A.C.; formal analysis, J.S.D., S.M.L., and M.P.;
572 investigation, J.S.D., P.J.M, S.M.L., M.P., and P.B.H.; resources, J.S.D., P.B.H., M.A.C., R.M.H, S.M.N, J.D.S.
573 and P.J.M.; data curation, J.S.D., S.M.L., P.J.M., and M.P.; writing—original draft preparation, J.S.D.;
574 writing—review and editing, J.S.D, M.A.C., P.J.M, S.M.L, M.P., P.B.H, R.M.H, S.M.N, J.D.S.; visualization,
575 J.S.D.; supervision, M.A.C.; project administration, M.A.C.; funding acquisition, M.A.C., P.J.M, R.M.H,
576 S.M.N, J.D.S..

577 *Conflicts of Interest:* The authors declare no conflict of interest. The funders had no role in the design of the
578 study; in the collection, analyses, or interpretation of data; in the writing of the manuscript, or in the decision
579 to publish the results.

580 *References*

581 Bartlett KB, Crill PM, Sass RL, et al (1992) Methane emissions from tundra environments in the Yukon-
582 Kuskokwim delta, Alaska. *J Geophys Res* 97:16645–16660. doi: 10.1029/91JD00610

583 Bastviken D, Cole J, Pace M, Tranvik L (2004) Methane emissions from lakes: Dependence of lake
584 characteristics, two regional assessments, and a global estimate. *Global Biogeochem Cycles* 18:1–12. doi:
585 10.1029/2004GB002238

586 Bastviken D, Cole JJ, Pace ML, Van de-Bogert MC (2008) Fates of methane from different lake habitats:
587 Connecting whole-lake budgets and CH₄ emissions. *J Geophys Res Biogeosciences* 113:G02024. doi:
588 10.1029/2007JG000608

589 Bastviken D, Ejlertsson J, Tranvik L (2002) Measurement of methane oxidation in lakes: A comparison of
590 methods. *Environ Sci Technol* 36:3354–3361. doi: 10.1021/es010311p

591 Beck AJ, Tsukamoto Y, Tovar-Sanchez A, et al (2007) Importance of geochemical transformations in
592 determining submarine groundwater discharge-derived trace metal and nutrient fluxes. *Appl*
593 *Geochemistry* 22:477–490. doi: 10.1016/J.APGEOCHEM.2006.10.005

594 Bring A, Fedorova I, Dibike Y, et al (2016) Arctic terrestrial hydrology: A synthesis of processes, regional
595 effects, and research challenges. *J Geophys Res Biogeosciences* 121:621–649. doi:
596 10.1002/2015JG003131

597 Brooks JR, Gibson JJ, Birks SJ, et al (2014) Stable isotope estimates of evaporation : inflow and water residence
598 time for lakes across the United States as a tool for national lake water quality assessments. *Limnol*
599 *Oceanogr* 59:2150–2165. doi: 10.4319/lo.2014.59.6.2150

600 Brown J, Ferrians Jr. OJ, Heginbottom JA, Melnikov ES (2002) Circum-Arctic Map of Permafrost and Ground-
601 Ice Conditions, version 2. National Snow and Ice Data Center

602 Burnett WC, Santos IR, Weinstein Y, et al (2007) Remaining uncertainties in the use of Rn-222 as a quantitative
603 tracer of submarine groundwater discharge. In: *IAHS-AISH Publication*. pp 109–118

604 Chanyotha S, Kranrod C, Burnett WC (2014) Assessing diffusive fluxes and pore water radon activities via a
605 single automated experiment. *J Radioanal Nucl Chem* 301:581–588. doi: 10.1007/s10967-014-3157-3

606 Chanyotha S, Kranrod C, Kritsanawanat R, et al (2016) Optimizing laboratory-based radon flux measurements
607 for sediments. *J Environ Radioact* 158–159:47–55. doi: 10.1016/j.jenvrad.2016.03.023

608 Charette M a, Moore WS, Burnett WC (2008) Uranium-and Thorium-Series Nuclides as Tracers of Submarine
609 Groundwater Discharge. *Radioact Environ* 13:155–191

610 Charette MA, Buesseler KO (2004) Submarine groundwater discharge of nutrients and copper to an urban

611 subestuary of Chesapeake Bay (Elizabeth River). *Limnol Oceanogr* 49:376–385. doi:
612 10.4319/lo.2004.49.2.0376

613 Charette MA, Buesseler KO, Andrews JE (2001) Utility of radium isotopes for evaluating the input and transport
614 of groundwater-derived nitrogen to a Cape Cod estuary. *Limnol Oceanogr* 46:465–470. doi:
615 10.4319/lo.2001.46.2.0465

616 Corbett DR, Burnett WC, Cable PH, Clark SB (1997) Radon tracing of groundwater input into Par Pond,
617 Savannah River Site. *J Hydrol* 203:209–227

618 Craig H (1961) Isotopic Variations in Meteoric Waters. *Science* (80-) 133:1702–1703. doi:
619 10.1126/science.133.3465.1702

620 Crawford JT, Striegl RG, Wickland KP, et al (2013) Emissions of carbon dioxide and methane from a headwater
621 stream network of interior Alaska. *J Geophys Res Biogeosciences* 118:482–494. doi: 10.1002/jgrg.20034

622 Crusius J, Wanninkhof R (2003) Gas transfer velocities measured at low wind speed over a lake. *Limnol*
623 *Oceanogr* 48:1010–1017. doi: 10.4319/lo.2003.48.3.1010

624 Dean JF, Middelburg JJ, Röckmann T, et al (2018) Methane Feedbacks to the Global Climate System in a
625 Warmer World. *Rev Geophys* 56:207–250. doi: 10.1002/2017RG000559

626 Dimova NT, Burnett WC (2011) Evaluation of groundwater discharge into small lakes based on the temporal
627 distribution of radon-222. *Limnol Oceanogr* 56:486–494. doi: 10.4319/lo.2011.56.2.0486

628 Dimova NT, Burnett WC, Chanton JP, Corbett JE (2013) Application of radon-222 to investigate groundwater
629 discharge into small shallow lakes. *J Hydrol* 486:112–122. doi: 10.1016/j.jhydrol.2013.01.043

630 Dimova NT, Paytan A, Kessler JD, et al (2015) Current Magnitude and Mechanisms of Groundwater Discharge
631 in the Arctic: Case Study from Alaska. *Environ Sci Technol* 49:12036–12043. doi:
632 10.1021/acs.est.5b02215

633 Dulaiova H, Camilli R, Henderson PB, Charette MA (2010) Coupled radon, methane and nitrate sensors for
634 large-scale assessment of groundwater discharge and non-point source pollution to coastal waters. *J*
635 *Environ Radioact* 101:553–563. doi: 10.1016/j.jenvrad.2009.12.004

636 Emerson SR, Hedges JI (2008) *Chemical Oceanography and the Marine Carbon Cycle*. Cambridge University
637 Press, New York

638 Ferrians Jr. OJ (1965) Permafrost map of Alaska. U.S. Geological Survey Miscellaneous Geologic
639 Investigations Map 445. Scale 1:2,500,000. 1

640 Fontes JC (1980) *Handbook of Environmental Isotope Geochemistry*. Elsevier Scientific Pub. Co., New York

641 Garcia-Tigreros Kodovska F, Sparrow KJ, Yvon-Lewis SA, et al (2016) Dissolved methane and carbon dioxide
642 fluxes in Subarctic and Arctic regions: Assessing measurement techniques and spatial gradients. *Earth*
643 *Planet Sci Lett* 436:43–55. doi: 10.1016/J.EPSL.2015.12.002

644 Gibson JJ, Birks SJ, Edwards TWD (2008) Global prediction of δA and δ^2H - $\delta^{18}O$ evaporation slopes for lakes
645 and soil water accounting for seasonality. *Global Biogeochem Cycles* 22:1–12. doi:
646 10.1029/2007GB002997

647 Gibson JJ, Edwards TWD, Birks SJ, et al (2005) Progress in isotope tracer hydrology in Canada. *Process*
648 19:303–327. doi: 10.1002/hyp.5766

649 Higuera PE, Chipman ML, Barnes JL, et al (2011) Variability of tundra fire regimes in Arctic Alaska:
650 Millennial-scale patterns and ecological implications. *Ecol Appl* 21:3211–3226. doi: 10.1890/11-0387.1

651 Holgerson MA, Raymond PA (2016) Large contribution to inland water CO₂ and CH₄ emissions from very
652 small ponds. *Nat Geosci* 9:222–226. doi: 10.1038/ngeo2654

653 Hornibrook ERC, Longstaffe FJ, Fyfe WS (1997) Spatial distribution of microbial methane production
654 pathways in temperate zone wetland soils: Stable carbon and hydrogen isotope evidence. *Geochim*
655 *Cosmochim Acta* 61:745–753. doi: 10.1016/S0016-7037(96)00368-7

656 Key RM, Brewer RL, Stockwell JH, et al (1979) Some improved techniques for measuring radon and radium
657 in marine sediments and in seawater. *Mar Chem* 7:251–264. doi: 10.1016/0304-4203(79)90042-2

658 Kim J, Kim G (2017) Inputs of humic fluorescent dissolved organic matter via submarine groundwater
659 discharge to coastal waters off a volcanic island (Jeju, Korea). *Sci Rep* 7:7921. doi: 10.1038/s41598-017-
660 08518-5

661 Kling GW, Kipphut GW, Miller MC (1992) The flux of CO₂ and CH₄ from lakes and rivers in arctic Alaska.
662 *Hydrobiologia* 23–36

663 Lecher A (2017) Groundwater Discharge in the Arctic: A Review of Studies and Implications for
664 Biogeochemistry. *Hydrology* 4:41. doi: 10.3390/hydrology4030041

665 Lehner B, Döll P (2004) Development and validation of a global database of lakes, reservoirs and wetlands. *J*
666 *Hydrol* 296:1–22. doi: 10.1016/J.JHYDROL.2004.03.028

667 Loranty MM, Lieberman-Cribbin W, Berner LT, et al (2016) Spatial variation in vegetation productivity trends,
668 fire disturbance, and soil carbon across arctic-boreal permafrost ecosystems. *Environ Res Lett* 11:. doi:
669 10.1088/1748-9326/11/9/095008

670 Ludwig S, Holmes RM, Natali SM, et al (2017a) Polaris Project 2017: Soil fluxes, carbon, and nitrogen, Yukon-

671 Kuskokwim Delta, Alaska

672 Ludwig S, Holmes RM, Natali SM, et al (2017b) Polaris Project 2017: Aquatic isotopes, carbon, and nitrogen,
673 Yukon-Kuskokwim Delta, Alaska

674 Ludwig S, Holmes RM, Natali SM, et al (2017c) Polaris Project 2017: Lake sediment carbon and nitrogen,
675 Yukon-Kuskokwim Delta, Alaska

676 Moore WS, Reid DF (1973) Extraction of radium from natural waters using manganese-impregnated acrylic
677 fibers. *J Geophys Res* 78:8880–8886. doi: 10.1029/JC078i036p08880

678 Morison MQ, Macrae ML, Petrone RM, Fishback L (2017a) Capturing temporal and spatial variability in the
679 chemistry of shallow permafrost ponds. *Biogeosciences* 14:5471–5485. doi: 10.5194/bg-14-5471-2017

680 Morison MQ, Macrae ML, Petrone RM, Fishback LA (2017b) Seasonal dynamics in shallow freshwater pond-
681 peatland hydrochemical interactions in a subarctic permafrost environment. *Hydrol Process* 31:462–475.
682 doi: 10.1002/hyp.11043

683 Natali SM, Schuur EAG, Mauritz M, et al (2015) Permafrost thaw and soil moisture driving CO₂ and CH₄
684 release from upland tundra. *J Geophys Res Biogeosciences* 120:1–13. doi:
685 10.1002/2014JG002872.Received

686 Paytan A, Lecher AL, Dimova N, et al (2015) Methane transport from the active layer to lakes in the Arctic
687 using Toolik Lake, Alaska, as a case study. *Proc Natl Acad Sci* 112:3636–3640. doi:
688 10.1073/pnas.1417392112

689 Paytan A, Shellenbarger GG, Street JH, et al (2006) Submarine groundwater discharge: An important source of
690 new inorganic nitrogen to coral reef ecosystems. *Limnol Oceanogr* 51:343–348. doi:
691 10.4319/lo.2006.51.1.0343

692 Rawlins MA, Steele M, Holland MM, et al (2010) Analysis of the Arctic System for Freshwater Cycle
693 Intensification: Observations and Expectations. *J Clim* 23:5715–5737. doi: 10.1175/2010JCLI3421.1

694 Richardson CM, Dulai H, Popp BN, et al (2017) Submarine groundwater discharge drives biogeochemistry in
695 two Hawaiian reefs. *Limnol Oceanogr* 62:S348–S363. doi: 10.1002/lno.10654

696 Sae-Lim J, Russell JM, Vachula RS, et al (2019) Temperature-controlled tundra fire severity and frequency
697 during the last millennium in the Yukon-Kuskokwim Delta, Alaska. *Holocene*. doi:
698 10.1177/0959683619838036

699 Schubert M, Paschke A, Bednorz D, et al (2012) Kinetics of the water/air phase transition of radon and its
700 implication on detection of radon-in-water concentrations: Practical assessment of different on-site radon

701 extraction methods. *Environ Sci Technol* 46:8945–8951. doi: 10.1021/es3019463

702 Schuur EAG, Bockheim J, Canadell JG, et al (2008) Vulnerability of Permafrost Carbon to Climate Change :
703 Implications for the Global Carbon Cycle. *Bioscience* 58:701–714

704 Schuur EAG, McGuire AD, Schädel C, et al (2015) Climate change and the permafrost carbon feedback. *Nature*
705 520:171–179. doi: 10.1038/nature14338

706 Sepulveda-Jauregui A, Walter Anthony KM, Martinez-Cruz K, et al (2015) Methane and carbon dioxide
707 emissions from 40 lakes along a north-south latitudinal transect in Alaska. *Biogeosciences* 12:3197–3223.
708 doi: 10.5194/bg-12-3197-2015

709 Throckmorton HM, Newman BD, Heikoop JM, et al (2016) Active layer hydrology in an arctic tundra
710 ecosystem: quantifying water sources and cycling using water stable isotopes. *Hydrol Process* 30:4972–
711 4986. doi: 10.1002/hyp.10883

712 US Fish & Wildlife Service (2002) Yukon Delta National Wildlife Refuge. In: Fact Sheet.
713 https://www.fws.gov/uploadedFiles/Region_7/NWRS/Zone_1/Yukon_Delta/PDF/yukondelta.pdf.
714 Accessed 24 Jul 2018

715 Vihma T, Screen J, Tjernström M, et al (2016) The atmospheric role in the Arctic water cycle: A review on
716 processes, past and future changes, and their impacts. *J Geophys Res Biogeosciences* 121:586–620. doi:
717 10.1002/2015JG003132

718 Vonk JE, Tank SE, Bowden WB, et al (2015) Reviews and syntheses: Effects of permafrost thaw on Arctic
719 aquatic ecosystems. *Biogeosciences* 12:7129–7167. doi: 10.5194/bg-12-7129-2015

720 Walter Anthony K, Schneider von Deimling T, Nitze I, et al (2018) 21st-century modeled permafrost carbon
721 emissions accelerated by abrupt thaw beneath lakes. *Nat Commun* 9:3262. doi: 10.1038/s41467-018-
722 05738-9

723 Walvoord MA, Kurylyk BL (2016) Hydrologic Impacts of Thawing Permafrost—A Review. *Vadose Zo J* 15:1–
724 20. doi: 10.2136/vzj2016.01.0010

725 Walvoord MA, Striegl RG (2007) Increased groundwater to stream discharge from permafrost thawing in the
726 Yukon River basin: Potential impacts on lateral export of carbon and nitrogen. *Geophys Res Lett* 34:. doi:
727 10.1029/2007GL030216

728 Wanninkhof R (1992) Relationship Between Wind Speed and Gas Exchange. *J Geophys Res* 97:7373–7382

729 Warwick NJ, Cain ML, Fisher R, et al (2016) Using $\delta^{13}\text{C-CH}_4$ and $\delta\text{D-CH}_4$ to constrain Arctic methane
730 emissions. *Atmos Chem Phys* 16:14891–14908. doi: 10.5194/acp-16-14891-2016

731 Whiticar MJ (1999) Carbon and hydrogen isotope systematics of bacterial formation and oxidation of methane.
732 Chem Geol 161:291–314. doi: 10.1016/S0009-2541(99)00092-3

733 Whiticar MJ, Faber E (1986) Methane oxidation in sediment and water column environments - Isotope evidence.
734 Org Geochem 10:759–768. doi: 10.1016/S0146-6380(86)80013-4

735 Wiesenburg DA, Guinasso NL (1979) Equilibrium solubilities of methane, carbon monoxide, and hydrogen in
736 water and sea water. J Chem Eng Data 24:356–360. doi: 10.1021/je60083a006

737 Wik M, Varner RK, Anthony KW, et al (2016) Climate-sensitive northern lakes and ponds are critical
738 components of methane release. Nat. Geosci. 9:99–105

739 Williams JR (1970) Ground water in the permafrost regions of Alaska

740 Wilson FH, Hults CP, Mull CG, Karl SM (2015) Geologic Map of Alaska. USGS Scientific Investigations Map
741 3340, pamphlet

742 Woo MK (2012) Permafrost hydrology. Springer

743 Wrona FJ, Johansson M, Culp JM, et al (2016) Transitions in Arctic ecosystems: Ecological implications of a
744 changing hydrologic regime. J Geophys Res Biogeosciences 121:650–674. doi: 10.1002/2015JG003133

745

Journal: Biogeochemistry

Title: Using radon to quantify groundwater discharge and methane fluxes to a shallow, tundra lake on the Yukon-Kuskokwim Delta, Alaska

Authors: Jessica S. Dabrowski ^{1,2*}, Matthew A. Charette, Paul J. Mann, Sarah M. Ludwig, Susan M. Natali, Robert Max Holmes, John D. Schade, Margaret Powell, and Paul B. Henderson

*Affiliation and correspondence: jsdabrow@mit.edu; Tel.: +01-508-289-3850

¹ Department of Earth and Planetary Sciences, Massachusetts Institute of Technology, 77 Massachusetts Ave, Cambridge, MA 02139, USA; jsdabrow@mit.edu, *ORCID:* 0000-0002-3196-4027;

² Department of Marine Chemistry & Geochemistry, Woods Hole Oceanographic Institution, 266 Woods Hole Road, MS#25, Woods Hole, MA 02543, USA; mcharette@whoi.edu; phenderson@whoi.edu;

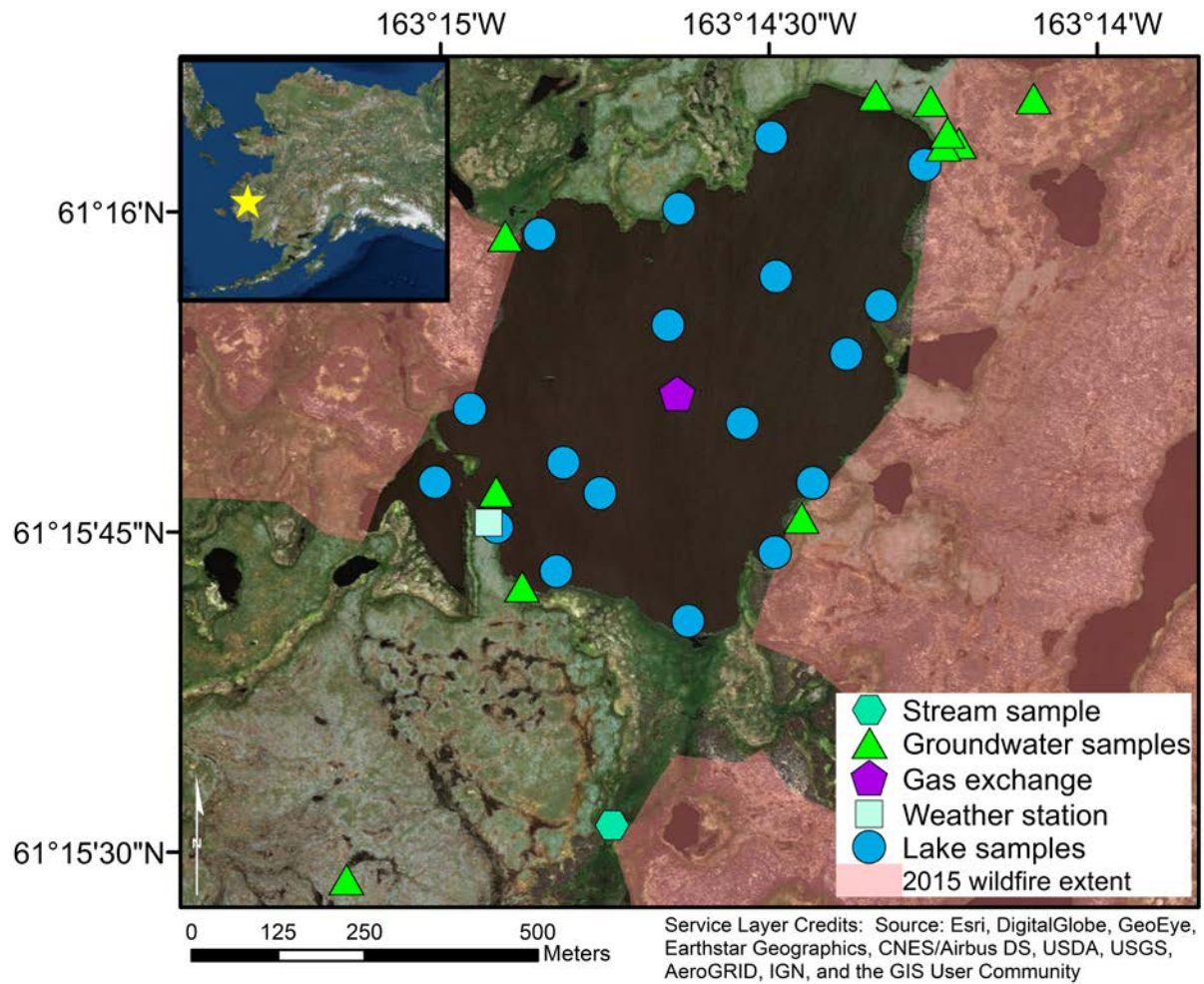


Fig. 1 “Landing Lake” sampling locations and the study site location within Alaska, USA shown in inset (star symbol). One groundwater sample (B2) is not shown because it was 5 km north of Landing Lake (Figure was made using ArcMap 10.5.1).

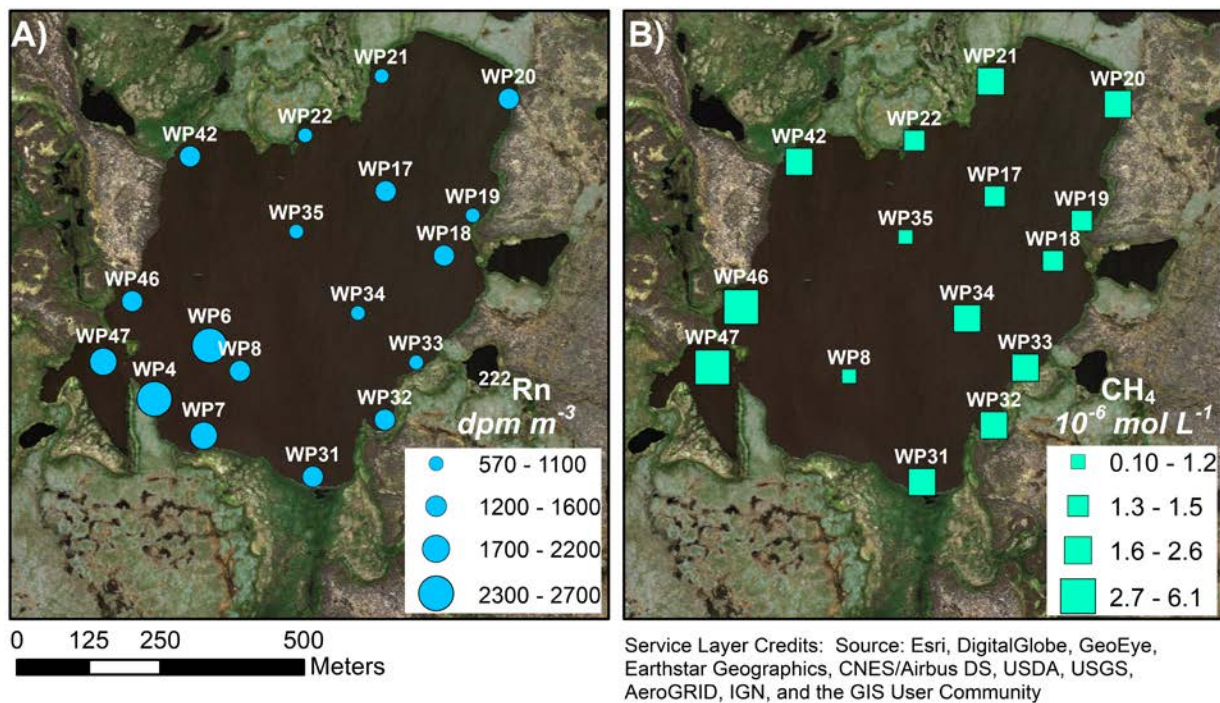


Fig. 2 Concentrations of (a) dissolved ^{222}Rn and (b) dissolved methane in Landing Lake. Sizes of symbols represent relative concentrations. CH_4 error = 30% for all samples; ^{222}Rn error = 16% for WP4, 0.1-6% for all other samples. (Figure was made using ArcMap 10.5.1).

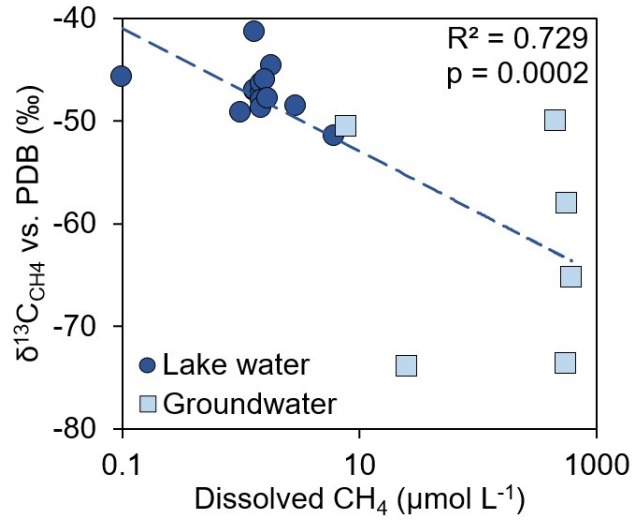


Fig. 3 Stable carbon isotopes of dissolved CH₄ as a function of CH₄ concentration in groundwater (light blue squares) and surface water samples (dark blue circles) at Landing Lake in 2017. Notice the logarithmic scale on the x-axis. The regression equation is $\delta^{13}\text{C} = -5.98 \log [\text{CH}_4, \mu\text{mol L}^{-1}] - 46.9\%$ and includes both the lake waters and groundwaters. PDB = Pee Dee Belemnite standard. (Figure made using Microsoft Excel).

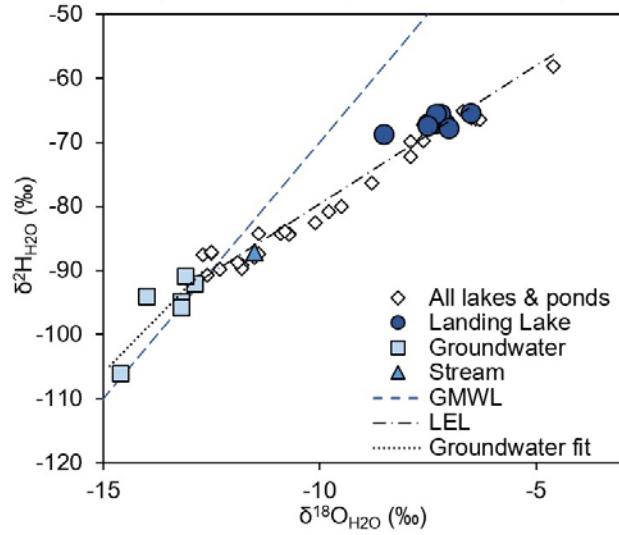


Fig. 4 The stable isotope values for $\delta^2\text{H}$ and $\delta^{18}\text{O}$ in water for samples collected in 2017. The stream sample (triangle) drains Landing Lake. The dashed line is the Global Meteoric Water Line (Craig 1961). Diamonds represent all lake and pond samples collected in 2017 (see data online: (Ludwig et al. 2017b)) which were fit with a Local Evaporation Line (LEL): $\delta^2\text{H}_{\text{H}_2\text{O}} = 4.31(\delta^{18}\text{O}) - 36.55\text{‰}$ ($R^2 = 0.96$, $p \ll 0.01$). The dotted black line is the best-fit line for Landing Lake groundwaters: $\delta^2\text{H}_{\text{H}_2\text{O}} = 6.87(\delta^{18}\text{O}) - 2.90\text{‰}$ ($R^2 = 0.70$, $p = 0.04$). (Figure made using Microsoft Excel).

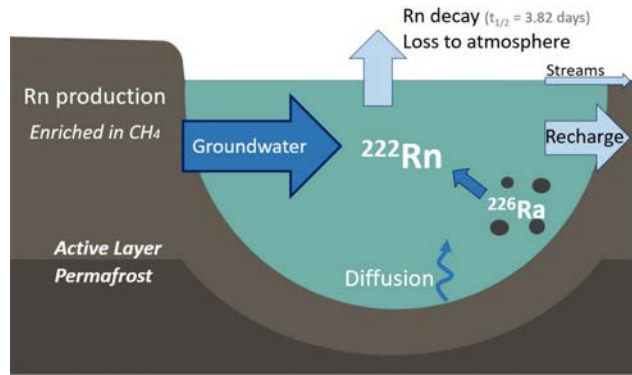


Fig. 5 A conceptual model showing the sources and sinks of ^{222}Rn in Landing Lake. Sources (dark blue arrows) include decay of dissolved ^{226}Ra in lake water, diffusion from lake bottom sediments and groundwater. Sinks (light blue arrows) include ^{222}Rn decay, loss to the atmosphere via gas exchange, recharge into soils, and the stream outlet. (Figure made using Microsoft Powerpoint).

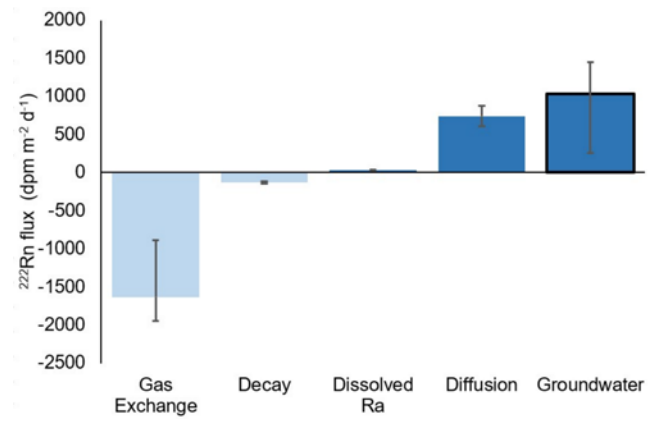


Fig. 6 The fluxes of ^{222}Rn for each source (dark blue) and sink (light blue) in the mass balance model for Landing Lake. The radon flux due to groundwater is highlighted with a black outline because it is the difference between the sinks and the other two sources. Error bars are propagated errors. Lower limits are the conservative estimate discussed in the text. (Figure made using Microsoft Excel).